Technische Universität München
TUM School of Engineering and Design

Data-Driven Analysis in the Cell Finalization of Lithium-ion Battery Production

Sandro Eugen Stock

Vollständiger Abdruck der von der TUM School of Engineering and Design der Technischen Universität München zur Erlangung eines

Doktors der Ingenieurwissenschaften (Dr.-Ing.)

genehmigten Dissertation.

Vorsitz: Prof. Dr.-Ing. Andreas Jossen

Prüfende der Dissertation:

1. Prof. Dr.-Ing. Rüdiger Daub
2. Prof. Dr.-Ing. Markus Lienkamp

Die Dissertation wurde am 03.02.2025 bei der Technischen Universität München eingereicht und durch die TUM School of Engineering and Design am 22.04.2025 angenommen.

Editors‘ Preface

In times of global challenges, such as climate change, the transformation of mobility, and an ongoing demographic change, production engineering is crucial for the sustainable advancement of our industrial society. The impact of manufacturing companies on the environment and society is highly dependent on the equipment and resources employed, the production processes applied, and the established manufacturing organization. The company’s full potential for corporate success can only be taken advantage of by optimizing the interaction between humans, operational structures, and technologies. The greatest attention must be paid to becoming as resource-saving, efficient, and resilient as possible to operate flexibly in the volatile production environment.

Remaining competitive while balancing the varying and often conflicting priorities of sustainability, complexity, cost, time, and quality requires constant thought, adaptation, and the development of new manufacturing structures. Thus, there is an essential need to reduce the complexity of products, manufacturing processes, and systems. Yet, at the same time, it is also vital to gain a better understanding and command of these aspects.

The research activities at the Institute for Machine Tools and Industrial Management (*iwb*) aim to continuously improve product development and manufacturing planning systems, manufacturing processes, and production facilities. A company’s organizational, manufacturing, and work structures, as well as the underlying systems for order processing, are developed under strict consideration of employee-related requirements and sustainability issues. However, the use of computer-aided and artificial intelligence-based methods and the necessary increasing degree of automation must not lead to inflexible and rigid work organization structures. Thus, questions concerning the optimal integration of ecological and social aspects in all planning and development processes are of utmost importance.

The volumes published in this book series reflect and report the results from the research conducted at *iwb*. Research areas covered span from the design and development of manufacturing systems to the application of technologies in manufacturing and assembly. The management and operation of manufacturing systems, quality assurance, availability, and autonomy are overarching topics affecting all areas of our research. In this series, the latest results and insights from our application-oriented research are published, and it is intended to improve knowledge transfer between academia and a wide industrial sector.

Rüdiger Daub *Gunther Reinhart* *Michael Zäh*

Preface

This dissertation was prepared during my time as a research associate at the Institute for Machine Tools and Industrial Management (*iwb*) at the Technical University of Munich (TUM). I am grateful for the opportunity to conduct my research in such a professional and inspiring environment.

First and foremost, I wish to express my sincere appreciation to Prof. Dr.-Ing. Rüdiger Daub for his expert supervision, valuable feedback, and steady support throughout all phases of this work. His clear guidance, constructive input, and reliability were instrumental in the successful completion of this dissertation. My thanks also go to Prof. Dr.-Ing. Gunther Reinhart and Prof. Dr.-Ing. Michael Zäh, whose leadership and commitment to academic excellence have shaped the *iwb* into an outstanding research environment. I am further grateful to Prof. Dr.-Ing. Markus Lienkamp for serving as co-advisor, and to Prof. Dr.-Ing. Andreas Jossen for chairing the defense.

I would like to thank my colleagues at *iwb* for their collaboration, technical insight, and team spirit. Working alongside such motivated and competent individuals made this journey both productive and enjoyable. Special recognition goes to Lucas Hille, Célestine Singer, and Jan Hagemeister for reviewing this dissertation, as well as for their valuable discussions and friendship. Their thoughtful input and steady support had a lasting impact, both academically and personally. I also extend my thanks to the students I had the privilege to supervise, whose dedication and contributions greatly enriched this research.

I am deeply thankful to my family and friends for their continuous encouragement. I especially thank my parents for providing a strong foundation of support, allowing me to pursue challenges with confidence. I am also grateful to Timo, whose advice and encouragement were crucial during my transition from physics into mechanical engineering. Finally, I would like to thank my fiancée Toni for the unwavering support throughout this journey. Your understanding, patience, and motivation, especially during difficult periods, helped me maintain perspective and resilience. Your presence and support were essential to this achievement.

Munich, July 2025 *Sandro Stock*

Table of Contents

List of Abbreviations

AC-IR	Alternating current internal resistance
AI	Artificial intelligence
ANN	Artificial neural network
BEV	Battery electric vehicle
CC	Constant current
CC-CV	Constant current, constant voltage
CEB	Cell expansion bracket
CEI	Cathode electrolyte interphase
C	Carbon
Co	Cobalt
CO	Carbon monoxide
CO_2	Carbon dioxide
CPS	Cyber-physical system
CRISP-DM	Cross-industry standard process for data mining
CV	Constant voltage
CH_4	Methane
C_2H_2	Acetylene
C_2H_4	Ethylene
C_2H_6	Ethane
C_3H_6	Propylene
C_3H_8	Propane
DC-IR	Direct current internal resistance
DEC	Diethyl carbonate
DEMS	Differential electrochemical mass spectrometry
DL	Deep learning

DMC	Dimethyl carbonate
DNN	Deep neural networks
DRM	Design research methodology
DVA	Differential voltage analysis
EC	Ethylene carbonate
ECM	Electrode equivalent circuit model
EIS	Electrochemical impedance spectroscopy
EMC	Ethyl methyl carbonate
EOL	End-of-line
ESA	Electrode-separator assembly
FCNN	Fully connected neural network
FEC	Fluoroethylene carbonate
GWRE	Gold-wire reference electrode
HF	Hydrofluoric acid
H_2	Hydrogen
ICA	Incremental capacity analysis
IM	Innovation module
iwb	Institute for Machine Tools and Industrial Management
KDD	Knowledge discovery in databases
LCO	Lithium cobalt oxide
LFP	Lithium iron phosphate
Li	Lithium
Li^+	Lithium ion
Li_2O	Lithium oxide
Li_2CO_3	Lithium carbonate
LIB	Lithium-ion battery
LIF	Lithium fluoride
$LiPF_6$	Lithium hexafluorophosphate
LNCO	Lithium nickel cobalt oxide

MAPE	Mean absolute percentage error
MI	Mutual information
Mg	Manganese
M_xO_y	Metal oxide
ML	Machine learning
NASA	National Aeronautics and Space Administration
NCA	Lithium nickel cobalt aluminum oxide
Ni	Nickel
NMC	Lithium nickel manganese cobalt oxide
NN	Neural network
OCV	Open-circuit voltage
OEMS	Online electrochemical mass spectrometry
O_2	Oxygen
OH^-	Hydroxide
P	Publication
PC	Propylene carbonate
PCC	Pearson's correlation coefficient
PHEV	Plug-in hybrid electric vehicle
ppm	parts per million
RBF	Radial basis function
ReLU	Rectified linear unit
RMSE	Root mean square error
$ROCO_2Li$	Lithium alkyl carbonates
RUL	Remaining useful lifetime
SEI	Solid-electrolyte interphase
Si-Gr	Silicon graphite
SLP	Single-layer pouch cell
SO	Scientific objective
SOC	State of charge

SOH	State of health
SVM	Support vector machines
SVR	Support vector regression
TUM	Technical University of Munich
VC	Vinylene carbonate
XPS	X-ray photoelectron spectroscopy
3D	Three-dimensional

List of Symbols

Lithium-ion battery

Symbol	Unit	Description
c_{AM}	Ah/kg	Specific capacity of active material
e	C	Elemental charge
e^-	-	Electron
E_{a}	V	Anode half-cell potential
E_{c}	V	Cathode half-cell potential
E_0	V	Open-circuit potential
I	I	Current
$\underline{I}$	I	Complex current
m_{AM}	kg	Mass of active material
Q	C	Capacity
Q_{c}	C	Charge capacity
Q_d	C	Discharge capacity
Q_{meas}	C	Measured capacity
Q_{theo}	C	Theoretical capacity
Q_{N}	C	Obtainable capacity
Q_0	C	Nominal capacity
R_{Ohm}	Ω	Ohmic resistance
t	s	Time
$\underline{U}$	V	Complex voltage
U	V	Cell voltage
U_0	V	Cell voltage in equilibrium
Z	Ω	Apparent resistance

$\underline{Z}$	Ω	Complex impedance
ϵ_C	-	Coulomb efficiency
ϕ	°	Phase shift
η	V	Overpotential

Machine learning

Symbol	Description
b_i	Bias
C	Regularization term
J	Cost function
n_{correct}	Correctly classified samples
n_{total}	Total samples
r^2	Regression coefficient
w_j	Weights
w_0	Bias
x_i	Input value / feature
y_i	Actual value
$\hat{y}_i$	Output value / predicted value
z	Weighted sum of inputs
ξ	Slack variable

1 Introduction

"Life is and will ever remain an equation incapable of solution,
but it contains certain known factors."
(Nikola Tesla, 1856 – 1943)

1.1 Motivation

Reducing anthropogenic greenhouse gas emissions is one of the biggest challenges for society in the 21st century (DIETZ ET AL. 2020). A promising approach for emission reduction involves the substitution of fossil fuels with renewable energy sources. Since renewable energy sources are subject to natural variations, energy storage solutions are required. In recent years, lithium-ion batteries (LIBs) emerged as highly promising energy storage solutions for stationary and mobile applications. Recognizing the significant impact of LIBs on society, Stanley Whittingham, John Goodenough, and Akira Yoshino were awarded the Nobel Prize in chemistry in 2019 for their contributions to LIB development (ROYAL SWEDISH ACADEMY OF SCIENCES 2019).

Since their initial commercialization by Sony in 1991, LIBs have gradually taken over the consumer market for portable electronic devices and have increasingly penetrated the individual mobility sector in recent years (XIE & LU 2020). The mobility sector plays a pivotal role, accounting for 14.3 % of direct greenhouse gas emissions (LAMB ET AL. 2021). Driven by governmental regulation and consumer demand, the development and production of battery electric vehicles (BEVs) is expected to increase rapidly over the next decade. LIBs have taken the predominant role in BEVs due to their high efficiency, reliability, and lifetime. (KWADE ET AL. 2018) Consequently, the demand for LIB is predicted to increase by approximately 33 % annually, mainly driven by the growing BEV market (FLEISCHMANN ET AL. 2023). However, the high costs of LIBs and safety concerns remain challenging to the widespread market penetration of BEVs.

A key challenge within the automotive industry is to enhance the quality of LIB while reducing their costs. The production of LIBs has a significant impact on both their costs and quality, as it is characterized by complex production processes. (KWADE ET AL. 2018) The cell finalization (also referred to as cell finishing or cell conditioning), which comprises the final production steps after the cell assembly, accounts for approximately 33 % of overall production costs (LIU ET AL. 2021) and high throughput times (WOOD ET AL. 2019). The formation as a critical step of cell finalization is decisive for the overall cell quality, and represents a significant lever for cost reduction since expensive plant equipment is required over several hours to complete the process (SCHOMBURG ET AL. 2024). During formation, the LIB is initially charged, and passivation layers are formed on the surface of the electrode particles, which is accompanied by

gas evolution. The passivation layers, such as the solid-electrolyte interphase (SEI), are essential for a long lifetime and safe operation of the LIB. The formation is considered completed when the passivation layers are sufficiently formed, and no more gas is produced. (AN ET AL. 2016) While some studies aimed at reducing the formation time by deploying fast formation procedures based on current as well as voltage adaptations (AN ET AL. 2017, DREES ET AL. 2023, LEE ET AL. 2004), approaches targeting the connection of gas evolution and SEI formation to improve the formation procedure are scarce.

Changes in the formation procedure require comprehensive quality assurance to ensure that the cell performance is not diminished (SCHOMBURG ET AL. 2024). While some quality measures, such as cell capacity, cell resistance, and rate capability, can be assessed immediately, cycle life analysis requires several months of testing. This results from the difficulty in assessing the SEI quality since an inferior SEI might only be detected by a decreased cycle life (DREES ET AL. 2023). Consequently, research targeting the development of the formation process is time intensive. A potential solution lies in developing data-driven approaches for cycle life prediction that could reduce the required testing time. However, methods for predicting battery cycle life have not been applied to expedite process development or to guarantee cell quality when modifying formation procedures. The challenge of determining formation procedures efficiently thus results in high throughput times that create a bottleneck in cell finalization and overall battery production (WOOD ET AL. 2019).

1.2 Objective

This dissertation aims at introducing novel approaches for tailoring formation procedures and enabling data-driven analysis methods for quality assurance with the overall goal of accelerating as well as securing process development in cell finalization. The formation is essential for well-performing and safe LIBs but is challenging to assess due to complex, material-dependent electrochemical reactions. To gain insights into these cell-internal processes that limit the necessary formation time, a novel device is required to observe the electrochemical reactions during SEI formation by tracking the gas evolution. The real-time tracking of gas evolution in large-format pouch cells could enable the tailoring of cell-specific formation protocols and the definition of criteria for minimum formation times. Multiple state-of-the-art cell chemistries and cell formats need to be examined to prove the transferability of the developed approach. Furthermore, quality assurance is required to ensure that the cell-specific formation protocols do not diminish the cell quality. Current cycle life analysis requires several months of testing, resulting in long observation times and deceleration of process development. A data-driven approach for cycle life prediction is thus needed to reduce the required observation time. The aim is to develop a simple methodology for quality prediction based on data sets exclusively from cell finalization, thereby obviating the necessity for comprehensive data acquisition throughout the entire production chain. Consequently, a comprehensive production concept is required that allows the tracking of various quality parameters during formation and cell finalization. Following the cross-industry standard process for data mining (CRISP-DM), a methodology needs to be proposed to establish an iterative and transferable framework for data

analysis and evaluation. Various data sources, feature sources, and feature extraction methods could then be examined to identify efficient approaches for quality assessment. The cycle life prediction methodology ultimately requires the employment during formation of multi-layer cells to verify the developed approach and derive the optimization potential.

1.3 Research methodology

The research methodology and structure of this dissertation are derived from the design research methodology (DRM) introduced by BLESSING & CHAKRABARTI (2009). The DRM provides a framework for knowledge-based research and can be divided into four steps: research clarification, a first descriptive study, a prescriptive study, and a second descriptive study. Figure 1.1 displays the steps of the research methodology, with the scope and the respective structure of the thesis divided into five chapters. The review-based research clarification is provided in the introduction in Chapter 1 and the fundamentals in Chapter 2. In the introduction, the relevance of this dissertation is motivated, and the objectives are defined. The fundamentals provide the theoretical foundation regarding LIBs and machine learning (ML). Chapter 3 contains the comprehensive descriptive study I that covers the significant scientific literature, including formation protocols, gas evolution detection methods, as well as approaches for the remaining useful lifetime (RUL) and cycle life prediction. The comprehensive prescriptive study includes the embedded publications I – IV in Chapter 4. Publication V and the discussion belong to the initial descriptive study II that also comprises the conclusion in Chapter 5, in which the key research findings are summarized, and an outlook is presented.

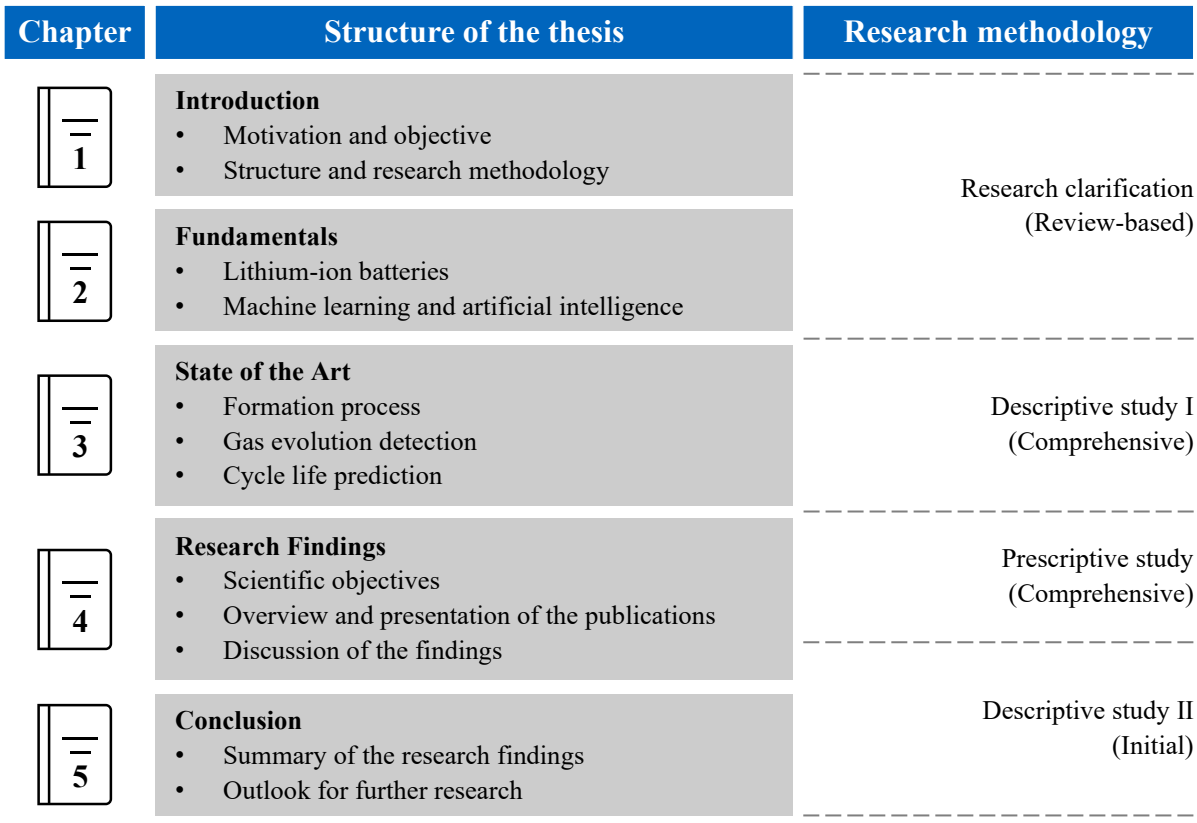

Figure 1.1: Overview of the thesis structure with the respective chapters and the research methodology derived from BLESSING & CHAKRABARTI (2009).

2 Fundamentals

In this chapter, the theoretical foundations for this thesis are explained. First, the fundamentals of LIBs are presented in Section 2.1, with emphasis on their structure, operating principle, production processes, as well as the formation and quality assurance within battery production. Subsequently, ML and artificial intelligence (AI) are addressed in Section 2.2, including an overview of ML methods, linear models, support vector models, and artificial neural networks (ANNs).

2.1 Lithium-ion batteries

LIBs are energy storage devices that store electrical energy as chemical energy through oxidation and reduction reactions. Since the conversion process from electrical to chemical energy is reversible, LIBs are classified as accumulators according to DIN 40729-05 (1985) and can consist of one or multiple cells. In this work, a LIB always refers to a single cell, and the terms battery and cell are used synonymously for LIBs.

2.1.1 Structure and operating principle

The main active components of a LIB are two different porous electrodes, an electrically insulating separator that separates the electrodes, and an ion-conducting electrolyte. Both electrodes consist of a current collector foil coated with a mixture of active materials, binding agents, electrically conductive agents, and additives. (LEUTHNER 2018, p. 14-15) Since reduction and oxidation occur at the different electrodes while charging and discharging, the terminology for LIBs is defined in the discharging state. Thus, the negative electrode in the discharging process is always referred to as anode, and the positive electrode as cathode (VUORILEHTO 2018, p. 22-23). Although different materials are needed for the energy conversion process, all LIBs utilize lithium ions (Li^+) for the charge transfer (LEUTHNER 2018, p. 13). Li^+ are reversibly stored in the active materials of the electrodes in an intercalation process during the interacting oxidation and reduction reactions. Intercalation describes accommodating Li^+ without causing structural damage in the active material. (VUORILEHTO 2018, p. 22-23)

Graphite is most frequently used as anode material for the Li^+ intercalation since it is abundant and relatively cheap. Li^+ are hereby stored between the graphene layers whereby a maximum lithiation of LiC_6 can be achieved, resulting in a specific capacity of 372 mAh/g. (WURM ET AL. 2018, p. 48) With a over ten-times higher specific capacity of up to 4200 mAh/g, silicon is becoming increasingly important as an anode active material but shows deficiencies regarding the cycle life (FENG ET AL. 2018).

A wide range of active materials are used for the cathode with layered lithium metal oxides, such as lithium nickel manganese cobalt oxide $Li_{1-x}(Ni_yCo_zMn_{1-(y+z)})O_2$ (NMC) or lithium nickel cobalt aluminum oxide $Li_{1-x}(Ni_yCo_zAl_{1-(y+z)})O_2$ (NCA), being among the most prominent (GRAF 2018, p. 30-33). The choice of the active material depends strongly on the application and affects several battery properties like energy density, fast charging capability, or cycle life. (ANDRE ET AL. 2015) Various conductive agents within both electrodes are used to increase the electric conductivity and binding agents are added to increase the cohesion within the electrodes, and the adhesion to the current collectors. Copper is commonly used for the anode current collector and aluminum for the cathode current collector. (VUORILEHTO 2018, p. 23)

The electrodes are electrically and mechanically separated by a separator, which has a microporous structure to allow Li^+ diffusion. Polymers like polyethylene and polypropylene are frequently used as separator materials. (WEBER & ROTH 2018, p. 78) The pores of the separator and the electrodes are filled with an ion-conducting liquid electrolyte consisting of a mixture of organic solvents, conducting lithium salts, and additives. In commercial cells, ether- and ester-based solvents are often used in which a conducting salt like lithium hexafluorophosphate ($LiPF_6$) is solved (HARTNIG & SCHMIDT 2018, p. 61-63). Furthermore, additives like vinylene carbonate (VC) are frequently added to the electrolyte to improve specific cell properties (AURBACH ET AL. 2002).

The basic structure of a LIB during discharging is presented in Figure 2.1, in which the main components are labeled. During discharging, Li^+ deintercalate from the anode active material (e.g., graphite) and migrate through the electrolyte as well as the separator to intercalate in the cathode active material (e.g., NMC) (LEUTHNER 2018, p. 14). An electron (e^-) conduction between the electrodes must be concurrently facilitated via an external circuit to provide charge neutrality within the electrodes. (KURZWEIL & DIETLMEIER 2018, p. 165-166) The discharge process represents a redox reaction due to the e^- transport, whereby the anode is oxidized, and the cathode is reduced.

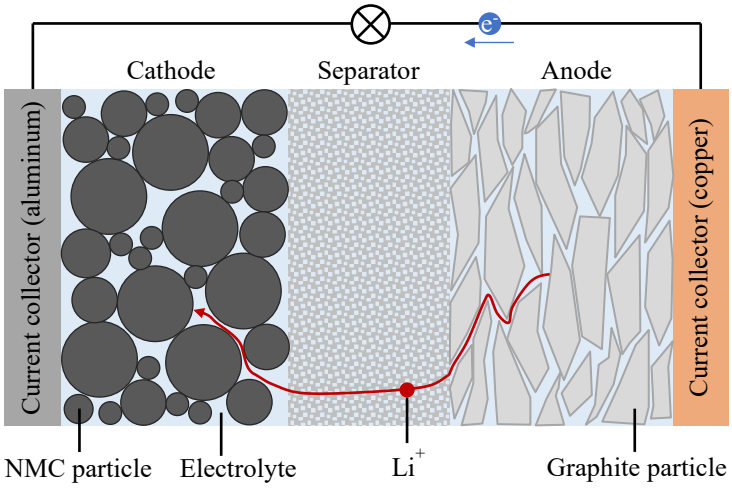

Figure 2.1: Schematic structure and operating principle of a LIB with a NMC cathode and graphite anode based on LEUTHNER (2018, p. 15). The Li^+ diffusion path (red) and e^- flow (blue) are displayed for the discharging process.

For the exemplary galvanic cell shown in Figure 2.1, the oxidation can be expressed as:

$$\mathrm{Li}_x\mathrm{C}_6 \rightarrow \mathrm{C}_6 + x\mathrm{Li}^+ + x\mathrm{e}^- \tag{2.1}$$

and the reduction as:

$$x\mathrm{Li}^+ + x\mathrm{e}^- + \mathrm{Li}_{1-x}\left(\mathrm{Ni}_y\mathrm{Co}_z\mathrm{Mn}_{1-(y+z)}\right)\mathrm{O}_2 \rightarrow \mathrm{Li}_x\left(\mathrm{Ni}_y\mathrm{Co}_z\mathrm{Mn}_{1-(y+z)}\right)\mathrm{O}_2 \tag{2.2}$$

with x denoting the number of Li^+, and y as well as z denoting the ratios of the metals in the active material. In the charging process, the redox reaction is reversed. (KURZWEIL & DIETLMEIER 2018, p. 166)

2.1.2 Parameters and definitions

The capacity Q of a battery indicates the amount of electrical charge that can be stored within the cell (charge capacity Q_c) or withdrawn from the cell (discharge capacity Q_d) and is defined as:

$$Q_\mathrm{c/d} = n \cdot \mathrm{e} \tag{2.3}$$

with n being an arbitrary number ($n \in \mathbb{N}$) and e the elemental charge. The ratio of discharge to charge capacity is called coulombic efficiency ϵ_C and is expressed as: (LEUTHNER 2018, p. 16)

$$\epsilon_\mathrm{C} = \frac{Q_\mathrm{d}}{Q_\mathrm{c}} \tag{2.4}$$

The theoretical capacity Q_theo is usually determined by the specific capacity of the cathode active material c_AM and its mass m_AM.

$$Q_\mathrm{theo} = c_\mathrm{AM} \cdot m_\mathrm{AM} \tag{2.5}$$

In contrast, the measured capacity Q_meas can be determined according to DIN EN IEC 62660-1 (2019) via the discharge of the cell at a defined current I over the discharge time t in respect to the starting time t_0.

$$Q_\mathrm{meas} = \int_{t_0}^{t} I(t)dt \tag{2.6}$$

The nominal capacity Q_0 is defined as the initial capacity that can be withdrawn at specified test conditions at the beginning of the service life. As an indicator for the obtainable cell capacity, the state of charge (SOC) is defined as the ratio of the removable capacity Q to the nominal capacity Q_0 under defined conditions (KURZWEIL & DIETLMEIER 2018, p. 233):

$$SOC = \frac{Q}{Q_0} \tag{2.7}$$

To compare the (dis)charging capabilities of LIBs with different Q_0, a universal indicator, the C-rate, at a constant current (CC) is defined:

$$\text{C-rate} = \frac{I}{Q_0} \tag{2.8}$$

The C-rate is usually stated in $x \cdot C$ or C/x (with $x \in \mathbb{R}$) and allows for a convenient and application-oriented comparison of LIBs with different nominal capacities (KURZWEIL & DIETLMEIER 2018, p. 233-234). Since LIBs degrade during operation, the obtainable capacity Q_N decreases in relation to Q_0 which is described using the state of health (SOH):

$$SOH = \frac{Q_\mathrm{N}}{Q_0} \tag{2.9}$$

The (electrical) potential describes the ability of an electrical field to perform work on an electrical charge. Lithium (Li) has a standard reduction potential against a hydrogen reference electrode of -3.04 V, which is the highest among all elements. (BRATSCH 1989) This high potential, in combination with its low density, makes it very suitable for energy storage applications. Both anode and cathode provide a half-cell potential, which depends on the active material and the Li concentration. The cell voltage in equilibrium U_0 results from the anode half-cell potential E_a and the cathode half-cell potential E_c and can be expressed as: (KURZWEIL & DIETLMEIER 2018, p. 42-44)

$$U_0 = E_\mathrm{c} - E_\mathrm{a} \tag{2.10}$$

In the absence of an electrical current and thermodynamic equilibrium, the cell voltage can also be defined as open-circuit voltage (OCV). However, if a current is applied, the cell voltage is affected by overpotentials η and the internal resistance (R_Ohm) within the battery cell. During discharging, this results in an effective cell voltage $U(I)$ that can be expressed as

$$U(I) = \big(E_\mathrm{c} - \eta_\mathrm{c}(I)\big) - \big(E_\mathrm{a} - \eta_\mathrm{a}(I)\big) - R_\mathrm{Ohm} \cdot I \tag{2.11}$$

whereby R_Ohm denotes the sum of ohmic resistances (KURZWEIL & DIETLMEIER 2018, p. 42-44). The ohmic resistances include electrolyte resistance, electric material resistances, and contact resistances. Overpotentials arise due to polarization effects at the electrode-electrolyte interfaces where Li^+ can accumulate. This accumulation depends on the interface properties and the applied current. As a result, voltage limits are reached faster causing a reduced obtainable cell capacity $Q_\mathrm{N} < Q_0$. (KURZWEIL & DIETLMEIER 2018, 231-134)

In the case of high overpotentials during charging, the anode potential E_a can fall below 0 V vs. Li/Li^+, resulting in lithium plating at the anode. Lithium plating describes the accumulation of metallic lithium at the anode surface. The plated lithium can then form dendrites that can penetrate the separator and thus pose a substantial safety hazard. (WALDMANN ET AL. 2018)

2.1.3 Production of lithium-ion batteries

The production of LIBs can be divided into three main process sections: electrode manufacturing, cell assembly, and cell finalization (KWADE ET AL. 2018). An overview of the process chain within the pilot production line at the Institute for Machine Tools and Industrial Management (*iwb*) of the Technical University of Munich (TUM) is presented in Figure 2.2 (REINHART ET AL. 2013). Since pouch cells produced at the pilot production line of the *iwb* are primarily used in this work, this production chain is used as a reference. However, the individual production steps might differ depending on the cell format and manufacturer.

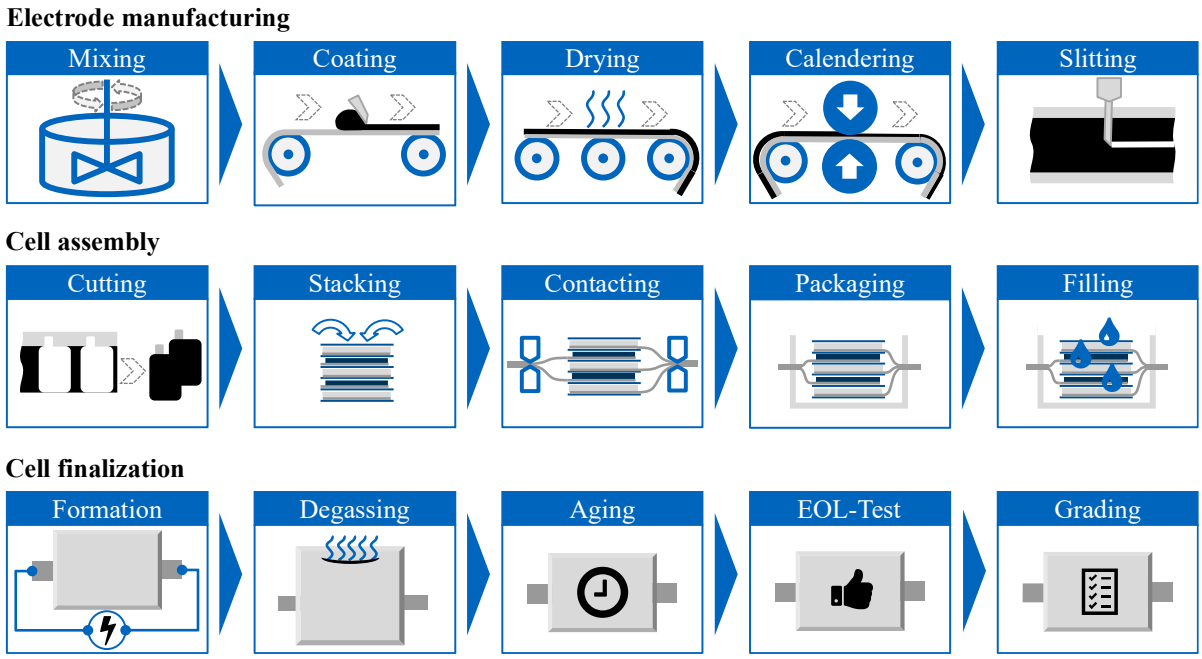

Figure 2.2: Schematic representation of the process chain for the production of LIBs separated in the main process sections: electrode manufacturing, cell assembly, and cell finalization.

The electrode manufacturing starts with mixing the electrode components and solvents into a homogenous mixture, the electrode slurry. A key objective is to obtain a slurry without agglomerates, which has a viscosity that allows further processing in the coating process. (KWADE ET AL. 2018) The slurry is continuously coated on a thin metallic foil, the current collector, using a slot die or doctor blade during the coating process (PETTINGER ET AL. 2018, p. 214). The coating thickness is used to influence the areal capacity of the electrode due to its dependence on the area-specific mass of the active material (i.e., the loading). In the subsequent drying process, the solvent added in the mixing is evaporated using a convection or infrared dryer. During calendering, the electrode coating is compacted under high pressure using two rollers to reduce the coating thickness and adjust the electrode porosity. (PETTINGER ET AL. 2018, p. 214-215) Depending on the cell format, the electrode coil is slitted into multiple coils with smaller widths. Afterward, the coils are dried under vacuum for several hours to reduce the moisture since cell assembly is usually performed inside a dry room. (HAWLEY & LI 2019)

Electrode sheets are cut from the coil using a laser in the first step of cell assembly. The cut electrode sheets, together with a separator, are further processed to form an electrode-separator assembly (ESA) in a stacking process. Z-folding is used to create the ESA by feeding a continuous separator in an alternating procedure around discrete electrodes. (KURFER ET AL. 2012) The single electrodes of the ESA are then joined using an ultrasonic welding process. For contacting, the uncoated current collector area of the electrode sheet is used. Conductor tabs are welded to the jointed current collectors which protrude out of the cell stack. (REINHART ET AL. 2013) Afterward, the cell is packaged into a housing to isolate the cell components from the environment. An aluminum-polymer composite foil is used for pouch cells, which is sealed on three sides by a heat-sealing process. One side remains open to enable an additional drying step and to allow for the electrolyte filling. (PETTINGER ET AL. 2018, p. 216-217) The electrolyte filling process can be divided into dosing and wetting. During dosing, the electrolyte is injected

into the cell and sealed in an evacuated state. To ensure a sufficient infiltration of the cell components with electrolyte, the packed cell is evacuated before dosing to remove residual air within the porous electrodes and separator. The electrolyte subsequently infiltrates and saturates the microporous structure of the electrodes and separator. (GÜNTER ET AL. 2019) This process takes several hours to ensure a complete wetting and the filled cells are usually stored in a heated chamber to reduce the viscosity of the electrolyte. (KWADE ET AL. 2018)

The cell finalization starts with the formation, in which the cell is charged for the first time. During formation, passivation layers are formed by electrochemical reactions that are essential for the safe and efficient operation of the LIB. (WOOD ET AL. 2019) This process is accompanied by gas evolution and is described in detail in Section 2.1.4 (SELF ET AL. 2015). The gases are pushed into a designated gas bag by applying an external pressure to the cell stack. Subsequently, the gases are removed by piercing a hole in the gas bag and applying an evacuation pressure. A final sealing is performed, and the gas bag is separated from the cell. (KWADE ET AL. 2018) To determine the cell quality, the LIB is stored and monitored at different temperatures for a defined period. Defective or minor-quality cells can be detected during the so-called aging by an increased self-discharge (YUE ET AL. 2017a). Finally, an EOL test is performed that includes different techniques to determine quality parameters like cell capacity, resistance, rate capability, or air tightness. The composition of the EOL test is strongly dependent on the manufacturer and the later application. (ANK ET AL. 2023) Detailed information on quality assurance is provided in Section 2.1.5. Finally, the LIBs are graded according to the quality parameters obtained in the EOL test, which marks the end of the production. (XIAOYU LI ET AL. 2014)

2.1.4 Formation of lithium-ion batteries

The formation is among the most time-intensive and quality-determining process steps in the production of LIBs (WOOD ET AL. 2015a). During formation, the cell is charged and discharged at low C-rates for the first time, which can take up to several hours or days. Hereby, passivation layers are formed, which are referred to as SEI at the anode and cathode electrolyte interphase (CEI) at the cathode. (WOOD ET AL. 2019) The SEI is a dense layer formed by reduction reactions of electrolyte components and Li^+ at the anode active material particles. The exact composition of the SEI is highly debated in literature and strongly material dependent. (AN ET AL. 2016) Commonly reported SEI components are Li_2CO_3 (AURBACH ET AL. 1996), $(CH_2OCO_2Li)_2$ (HEISKANEN ET AL. 2019), Li_2O (BAR‐TOW ET AL. 1999), LiF (PELED ET AL. 1998), and $ROCO_2Li$ (PELED ET AL. 1998), amongst others (AN ET AL. 2016, KIM ET AL. 2011, LU ET AL. 2014, WANG ET AL. 2018). Inorganic components are formed by reduction products of the lithium salt (e.g., $LiPF_6$) and are predominantly located close to the active material. Organic components arise from electrolyte solvent reduction and form the outer SEI at the electrolyte boundary. (AN ET AL. 2016)

SEI properties

The SEI enables the efficient operation of a LIB since it impedes further electrolyte decomposition and Li^+ consumption. Moreover, Li^+ form cation solvent adducts (solvate shells) in polar organic solvents that can be desolvated when passing through the SEI (HARTNIG &

SCHMIDT 2018, p. 67-68). The SEI causes the attached solvent molecules to strip from the Li^+, thus enabling intercalation of the sole Li^+ and preventing structural damage within the active material. In operation, the expansion of the graphene layers and the subsequent delamination of graphite are precluded by the SEI. (HARTNIG & SCHMIDT 2018, p. 70)

Functional requirements for a high-quality SEI include a complete and homogeneous composition, high permeability for Li^+, high diffusion resistance for electrolyte solvents, low electric conductivity, mechanical stability, and flexibility (KWADE ET AL. 2018). Flexibility is needed to compensate for the expansion and contraction of the anode active material particles during charging and discharging. Moreover, stability of the SEI over the applied potential and temperature range is required for the stable operation of the LIB. (WANG ET AL. 2018) The choice of the organic solvent strongly influences the SEI composition and properties. Ethylene carbonate (EC) has been reported to be beneficial for the formation of a high-quality SEI and is used in most electrolytes. (JEONG ET AL. 2001) However, EC has a melting point of 34 °C and is solid at room temperature. Thus, a combination with ethyl methyl carbonate (EMC), diethyl carbonate (DEC), or dimethyl carbonate (DMC) is often chosen to dissolve the EC and provide a liquid electrolyte at lower temperatures. (AN ET AL. 2016)

Additives are usually added to the electrolyte to influence specific properties of the SEI and LIB (ZHANG 2006). VC is frequently used to alter the SEI composition and improve cycling and thermal stability (BURNS ET AL. 2013). VC has a lower activation energy and is reduced before EC during the initial charging. This allows for an earlier intercalation of Li^+ and reduces the initial capacity loss (XU 2004). Lithium bis(oxalate)borate is often combined with VC and improves thermal stability during operation. For silicon graphite (Si-Gr) blend anodes, fluoroethylene carbonate (FEC) has been reported to improve cycling stability due to better flexibility and mechanical stability of the SEI. (ZHANG 2006) However, the choice of suitable additives depends strongly on the electrode materials, conducting salts, solvents, and operating conditions and is subject to intense research. A comprehensive study on the influence of additives on SEI formation using electrochemical impedance spectroscopy (EIS) revealed different SEI resistances depending on the applied additives (SOLCHENBACH ET AL. 2021). This influences the fast charging and aging behavior of the LIB.

From a production perspective, the influence on the SEI during formation is limited to the selection of the formation protocol, ambient temperature, and normal stress on the cell. The formation protocol describes the current and voltage profiles that are applied to the cell. Low C-rates are generally recommended to ensure a kinetically unrestricted, homogeneous, thin, and complete SEI formation while preventing lithium plating. (AN ET AL. 2016)

Gas evolution

There are numerous chemical and electrochemical reaction paths inside a LIB that cause gas evolution. Figure 2.3 provides an overview of selected reaction paths, including oxidation and reduction reactions, phase transformations, hydrolysis, and decomposition reactions.

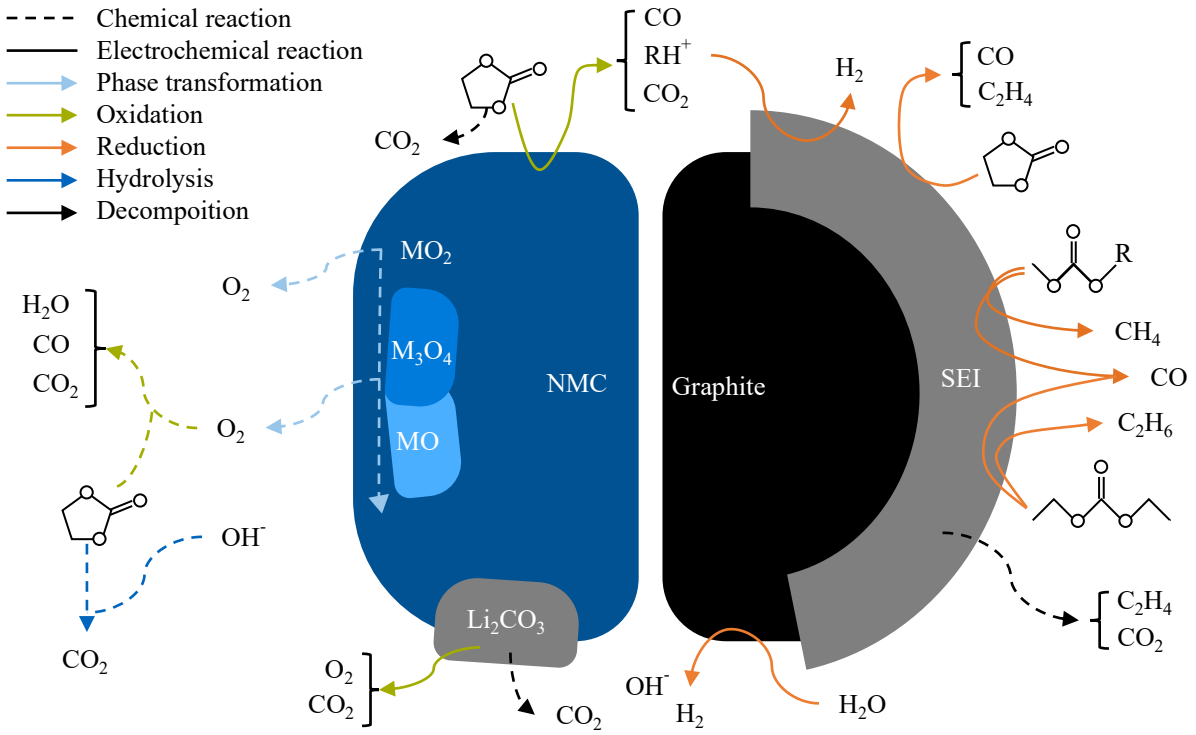

Figure 2.3: Main reaction mechanisms in a NMC/graphite LIB that lead to gas evolution (adapted from SALOMEZ ET AL. (2023)). The arrow type and color present different types of chemical and electrochemical reactions. A bracket indicates that several reaction products are possible.

The formation of the SEI is accompanied by the evolution of several gases like carbon monoxide (CO) and ethylene (C_2H_4) as well as linear carbonates like methane (CH_4), ethane (C_2H_6), and propane (C_3H_8) (SALOMEZ ET AL. 2023). These gases originate from decomposition (black arrow in Figure 2.3) or reduction of the electrolyte (orange arrow in Figure 2.3) at both electrodes in various voltage ranges. C_2H_4 is the most commonly emitted gas that originates following EC reduction at anode potentials $E_a < 1$ V vs. Li/Li$^+$ (ONUKI ET AL. 2008). Linear carbonates are reduced at $E_a < 0.9$ V vs. Li/Li$^+$ from either EMC, DEC, or DMC (SALOMEZ ET AL. 2023). CO can be generated by a reduction of cyclic as well as linear carbonates (ROWDEN & GARCIA-ARAEZ 2020).

Furthermore, gases can be produced at the cathode at high potentials by either electrochemical oxidation (green arrow in Figure 2.3) on the cathode active material surface or chemical oxidation by releasing oxygen from the cathode (MAO ET AL. 2019). The oxygen release during phase transitions (light blue arrow in Figure 2.3) is reported at potentials $E_c > 4.3$ vs. Li/Li$^+$ for NMC, whereby a further reaction to CO or carbon dioxide (CO_2) is likely (STREICH ET AL. 2017). The electrochemical oxidation can immediately generate CO and CO_2, but at higher potentials $E_c > 4.3$ vs. Li/Li$^+$. Besides high voltages, the oxygen release can also be triggered by high currents, high temperatures, cathode morphology changes, or impurities like water. (SALOMEZ ET AL. 2023)

Although water is not desired within the cell, mainly due to the reaction with the conductive salt $LiPF_6$ to form hydrofluoric acid (HF), a water concentration of 0 ppm is hardly possible, and reactions of the SEI with water must be considered as well (BERNHARD ET AL. 2015b).

Water can be reduced at a potential E_a < 1.3 V vs. Li/Li^+ to form reactive hydroxide (OH^-) radicals and hydrogen (H_2) (IMHOF & NOVÁK 1998). OH^- radicals, as well as water, can, in turn, react with EC to form CO_2 (dark blue arrow in Figure 2.3). However, the reaction with water requires temperatures above 60 °C, whereas OH^- reacts at room temperature (METZGER ET AL. 2016). Further side reactions that produce the aforementioned gases are cathode surface species, electrolyte degradation, or cross-talk reactions (HARRIS ET AL. 2020). Since these effects are caused by material impurities or degradation, their influence is difficult to assess during formation.

In summary, various gases evolve in the cell either by SEI-forming reactions, cathode-related oxygen release, or reactions due to impurities. However, the number of gases is limited, and some reactions only occur in specific voltage ranges, allowing for differentiation of cell internal processes by gassing analysis. (MICHALAK ET AL. 2015)

2.1.5 Quality assurance in cell finalization

Quality assurance during battery production is crucial to ensure a safe LIB operation throughout the entire service life. Insufficient cell quality can result from a multitude of factors, such as material defects, production errors, or stochastic variations in manufacturing. (SCHNELL & REINHART 2016) Stochastic variations caused by slight deviations in the bulk material, machine wear, or environmental conditions (e.g., temperature or humidity) are particularly difficult to detect as minor variations might be inconspicuous within the intermediate product properties (XIE ET AL. 2020). However, these variations can accumulate and result in deviations in quality parameters or defects in the final product (DUBARRY ET AL. 2010).

A quality assurance process step, known as the EOL test, is usually performed as the final process step in battery production (cf. Figure 2.2). The EOL test comprises different measurements to determine the quality parameters of the LIB and represents the final quality control before distribution to the customer. Quality parameters include the cell capacity, impedance, self-discharge, insulation, dimensions, and tightness. The quality assurance measures can be separated into electrical and non-electrical tests. (KWADE ET AL. 2018)

Electrical tests include resistance measurements using either a direct current internal resistance (DC-IR) measurement, an alternating current internal resistance (AC-IR) measurement, or both. The AC-IR measurement can either be performed at a single frequency or over multiple frequencies. Often, the resistance measurements are performed at different SOCs. (ANK ET AL. 2023) The self-discharge is usually determined in an aging process, in which the cell is stored at a defined temperature and regularly checked. Self-discharge causes a leakage current, and defective cells can be detected by either a high voltage drop or high leakage current. (YUE ET AL. 2017b) However, a measuring time of up to three weeks is necessary for accurate results (WOOD ET AL. 2015a). A capacity check using a charge and discharge cycle can also be performed during the EOL test but is often omitted since the capacity is determined in the prior formation step (ANK ET AL. 2023).

Non-electrical tests include optical inspections to detect welding defects as well as errors or irregularities in the cell housing (KWADE ET AL. 2018). For pouch cells, the emphasis is on the sealing quality and air tightness since the pouch foil provides less mechanical stability than a metal casing. Moreover, the weight and cell dimensions are checked in detail to provide a precise integration into the battery pack. These quality measurement techniques are specified in standards like the DIN EN IEC 62660-1 (DIN EN IEC 62660-1).

Additional measurement techniques are used in research to determine cell quality parameters. The EIS is often used to provide in-depth information regarding cell impedance (LAMBERT ET AL. 2017). EIS measurements are conducted using either an alternating voltage (potentiostatic EIS) or alternating current (galvanostatic EIS) excitation signal, and the respective current or voltage response is recorded (DIN EN ISO 16773-1). The complex impedance $\underline{Z}$ describes the frequency-dependent AC-IR of an electrical system and is defined as

$$\underline{Z} = \frac{\underline{U}}{\underline{I}} = Ze^{\mathrm{i}\phi} = Z\cos(\phi) + \mathrm{i}\,Z\sin(\phi) = \mathrm{Re}(\underline{Z}) + \mathrm{i}\,\mathrm{Im}(\underline{Z}) \tag{2.12}$$

with $\underline{U}$ denoting the complex alternating voltage, $\underline{I}$ the complex alternating current, ϕ the phase shift angle of the voltage in relation to the current, and Z the apparent resistance. The apparent resistance is defined as the ratio of the effective amplitudes of voltage to current. The expression can be written in different expressions using Euler's formula and split into a real resistance $\mathrm{Re}(\underline{Z})$ and a complex reactance $\mathrm{Im}(\underline{Z})$, which can then be displayed in a Nyquist plot. Applying an equivalent circuit model (ECM) to the impedance data allows the modeling of different components within the LIB and the derivation of various properties. Detailed information regarding ECMs is provided by LANDESFEIND ET AL. (2017) and PRITZL ET AL. (2018).

Further non-destructive measurement techniques that are less relevant for this work include image-based methods (e.g., computer tomography), acoustic methods (e.g., ultrasound), and calorimetric methods (e.g., isothermal calorimetry).

2.2 Machine learning and artificial intelligence

ML and AI have become integral to research across various disciplines, leveraging their ability to analyze comprehensive datasets, detect patterns, and reveal correlations. This section provides an overview of ML methods with an emphasis on linear and support vector models as well as ANNs.

2.2.1 Overview of machine learning methods

The idea of AI emerged in the mid-20$^{\text{th}}$ century when pioneers like Alan Turing envisioned machines that could "think" like humans and perform complex tasks (TURING 1950). Therefore, AI can be seen as an overarching term for systems, such as ML and deep learning (DL), that learn from inputs without explicit programming. DL is a specific area of ML that targets a broader range of data resources and often requires less data pre-processing, thus reducing the manual effort compared to other ML approaches (JOSHI 2020, p. 117).

The ML approach, which is primarily used in this work, gets predominantly trained instead of explicitly programmed, in contrast to conventional programming methods. Accordingly, the system can establish rules required for modeling a problem automatically. This is particularly helpful when analyzing complex problems and large data sets. (REBALA ET AL. 2019, p. 1-2) There are different types of ML approaches, which can be classified into four categories: supervised learning, unsupervised learning, semi-supervised learning, and reinforced learning (GÉRON 2019, p. 8):

- **Supervised learning:** The complete dataset of input and output values is given in supervised learning, whereby the outputs are called labels. The goal of the ML algorithm is the determination of an optimum function that maps the inputs to the labels. This process is called labeling or training, and the trained function can then be used on a new input to predict further labels. (JOSHI 2020, p. 10)

- **Unsupervised learning:** Unsupervised learning does not require labels, and the goal of the ML algorithm is to identify patterns and similarities within the given input data. This approach is frequently used to cluster samples or find inherent correlations within a data set. (JOSHI 2020, p. 11)

- **Semi-supervised learning:** In semi-supervised learning, a combination of unsupervised and supervised algorithms is applied. Complete labeling is thus not required, and algorithms are used that can cope with partially labeled training data. (GÉRON 2019, p. 13)

- **Reinforcement learning:** Reinforcement learning describes a self-learning system (called agent), which does not require input or output values. The agent learns from the environment and executes actions based on the observations. A reward or penalty is given to the ML algorithm during learning using a reward function, and the goal is to find a strategy to maximize the reward. Accordingly, the agent decides on actions that lead to a higher reward through past feedback. (GÉRON 2019, p. 13)

In this work, supervised learning models are utilized since all input values (e.g., characteristics during formation) can be mapped to labels (e.g., cycle life). Supervised learning can be used to solve both regression and classification tasks. For regression tasks, the output values (also referred to as labels or target values) are continuous variables. Classification tasks have discrete variables as output values, separated into two or more classes (or groups). Depending on the task as well as the relation between input and output values, different linear or nonlinear models are favorable. (REBALA ET AL. 2019, p. 20)

The overall process of using ML approaches to extract knowledge from data sources is frequently referred to as knowledge discovery in databases (KDD) (FROCHTE 2019, p. 15-17). A similar methodology is CRISP-DM, which provides a holistic methodology and simple transferability across industries. Figure 2.4 shows the overview of CRISP-DM with the iterative steps: business understanding, data understanding, data preparation, modeling, evaluation, and deployment. Business and data understanding provide the baseline for finding a suitable ML approach. Data preparation includes the selection, pre-processing, and transformation of the available data to be used in the modeling step. During modeling, different algorithms can be

applied to identify relationships within the data set. Based on the evaluation of the modeling results, the process is usually repeated several times before measures are deployed. (CHAPMAN ET AL. 2000)

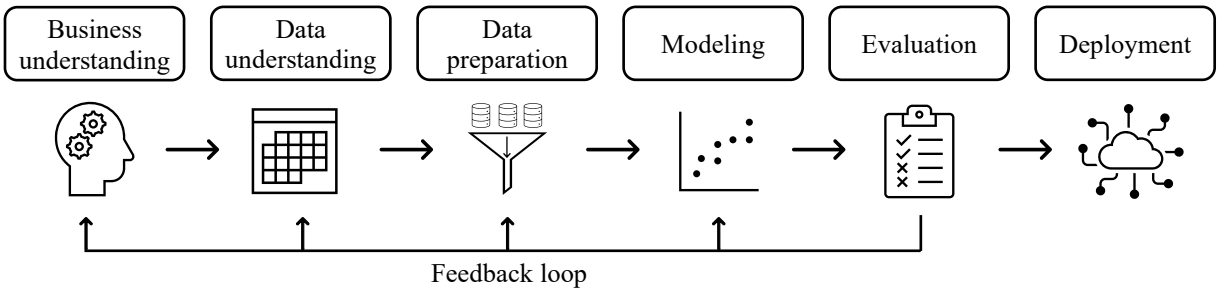

Figure 2.4: Representation of the individual steps within the CRISP-DM (adapted from CHAPMAN ET AL. 2020).

2.2.2 Linear and generalized linear regression

Regression analysis is a statistical method to assess relationships between one or more independent (input) values and a dependent (output) value (JOSHI 2020, p. 34). Linear regression provides a simple regression model that predicts a continuous output value $\hat{y}_\mathrm{i}$ using an input vector $\boldsymbol{x}$. The input variables x_i are referred to as features, and different weights w_j are assigned to each feature. For n features and $\hat{y}_\mathrm{i}$ output values, the expression can be written as:

$$\hat{y}_\mathrm{i} = w_0 + \sum_{\mathrm{j}=1}^{\mathrm{n}} w_\mathrm{j} x_{\mathrm{i,j}} \tag{2.13}$$

with w_0 denoting a bias term. (JOSHI 2020, p. 34) The linear regression algorithm adjusts the weights to minimize the deviation between the actual value y_i and predicted value $\hat{y}_\mathrm{i}$. This process is referred to as training of the model. Minimization of the mean squared error:

$$\min \|y_\mathrm{i} - \hat{y}_\mathrm{i}\| \tag{2.14}$$

is commonly used during training as it provides an unbiased estimate (JOSHI 2020, p. 35). The optimum weights can then be determined by applying Equation (2.13) in Equation (2.14) and solved using the cost function $J(w)$, which can be expressed as:

$$J(w) = \frac{1}{2m} \sum_{\mathrm{i}=1}^{\mathrm{m}} (\hat{y}_\mathrm{i}(x_\mathrm{i}) - y_\mathrm{i})^2 \tag{2.15}$$

with m being a natural number ($m \in \mathbb{N}$) (REBALA ET AL. 2019, p. 30). The cost function can be resolved using a normal equation or gradient descent. The normal equation is analytically solvable but requires high computational power if a large number of features are used. Gradient descent offers a simple iterative method in which the partial derivative of the cost function is used to approach the minimum. Reaching a global minimum can be ensured since the cost function is quadratic, however, a suitable learning rate must be chosen to ensure the convergence of the algorithm. (REBALA ET AL. 2019, p. 32-35)

Linear regression is preferably used if the input and output values have a linear relation. However, generalized linear models can also be applied to nonlinear relations but require prior transformation, referred to as basis or link function. (JOSHI 2020, p. 37) The basis function converts nonlinear relations between input and output to linear relations that can be used in linear regression. Classification tasks can be solved by selecting a logistic function $g(z_\mathrm{i})$ as a basis function to transform continuous variables z_i from a linear relation to a binary class: (JOSHI 2020, p. 37-38)

$$g(z_\mathrm{i}) = \frac{1}{1 + e^{z_\mathrm{i}}} \tag{2.16}$$

$$z_i = w_0 + \sum_{\mathrm{j}=1}^{\mathrm{n}} w_\mathrm{j} x_{\mathrm{i,j}} \tag{2.17}$$

The predicted binary value thus depends on the results from the transformation and is 0 if $g(z_\mathrm{i}) < 0.5$ and 1 if $g(z_\mathrm{i}) > 0.5$. Analog to linear regression, a modified cost function $J^*(w)$ can be defined for logistic regression to determine the optimum weights: (REBALA ET AL. 2019, p. 38)

$$J^*(w) = \frac{-1}{\mathrm{m}} \sum_{\mathrm{i}=1}^{\mathrm{m}} \big(y_\mathrm{i} \log(g(z_\mathrm{i})) - (1 - y_\mathrm{i}) \log\big(1 - g(z_\mathrm{i})\big) \big) \tag{2.18}$$

The modified cost function is non-convex and can not be solved using the normal equation method. Consequently, gradient descent is usually used to approach a minimum and find the optimum weights. (REBALA ET AL. 2019, p. 35-38)

To measure the performance of a model, the capability of predicting target values from input data that was not used during training is evaluated. Statistical metrics to measure the performance of regression models include the root mean square error (RMSE) and the mean absolute percentage error (MAPE), shown in Equation (2.19) and (2.20). (JOSHI 2020, p. 170-171)

$$RMSE = \sqrt{\frac{1}{n} \sum_{\mathrm{i}=1}^{\mathrm{n}} |\hat{y}_\mathrm{i} - y_\mathrm{i}|} \tag{2.19}$$

$$MAPE = \frac{1}{n} \sum_{\mathrm{i}=1}^{\mathrm{n}} \frac{|\hat{y}_\mathrm{i} - y_\mathrm{i}|}{y_\mathrm{i}} \cdot 100 \tag{2.20}$$

For classification models, accuracy is used to evaluate the model performance by taking the ratio of correctly classified samples n_correct to the total number of samples n_total: (JOSHI 2020, p. 171)

$$Accuracy = \frac{n_\mathrm{correct}}{n_\mathrm{total}} \tag{2.21}$$

The objective in training is to find ideal weights to maximize the generalization capability and ensure the best performance when testing new, unseen data sets. Cross-validation is a frequently

applied technique during training to improve generalization. By splitting the data set into subsets (e.g., by k-fold cross-validation), a performance evaluation within the training is achieved, which can improve the tuning of weights and the overall model performance. (REBALA ET AL. 2019, p. 53-54)

2.2.3 Support vector machines and support vector regression

Support vector machines (SVMs) were developed to solve classification and regression tasks regarding linearly as well as nonlinearly separable data sets (CORTES & VAPNIK 1995). The aim of the SVM is to maximize the margin between data points of different classes using a hyperplane (GÉRON 2019, p. 155-156). The hyperplane separating two classes can be defined as the set of points $\boldsymbol{x}$ that satisfy the equation

$$(\boldsymbol{w} \cdot \boldsymbol{x}) - w_0 = 0 \tag{2.22}$$

with $\boldsymbol{w}$ denoting the weight vector and w_0 the bias. Support vectors are hereby used to maximize the margin between the hyperplane and the data points from each class. An example of two linearly separable data sets is shown in Figure 2.5. (Decision) boundaries are defined such that values located at the "positive" side of the decision boundary (circles) have a value > 1 and at the "negative" side (crosses) a value ≤ 1. (JOSHI 2020, p. 67-68)

$$(\boldsymbol{w} \cdot x_\mathrm{i}) - w_0 \begin{cases} > 1, & \text{if } y_\mathrm{i} = 1 \\ \leq 1, & \text{if } y_\mathrm{i} = -1 \end{cases} \tag{2.23}$$

The distance between the two (decision) boundaries can be calculated using vector geometry and is expressed as

$$\frac{2}{\|\boldsymbol{w}\|} \tag{2.24}$$

with $\|\boldsymbol{w}\|$ denoting the Euclidean norm of the weight vector. The goal is thus to minimize $\|\boldsymbol{w}\|$ in order to maximize the margin while assuring that the condition defined in Equation (2.13) is fulfilled. Since most data sets are not entirely separable, a soft margin is introduced that allows several data points to violate the margin condition (i.e., allows data points to be located outside the decision boundaries or within the other class). For this, a penalty term is added to the optimization problem, resulting in: (JOSHI 2020, p. 69)

$$\min_{w,w_0} \frac{1}{2} \|\boldsymbol{w}^2\| + C \sum_{\mathrm{i}=1}^{\mathrm{m}} \xi_\mathrm{i} \tag{2.25}$$

with ξ_i denoting the so-called slack variable and C a regularization term. The optimization is frequently solved using its Lagrangian dual and is described in detail in FROCHTE (2019).

For support vector regression (SVR), a hyperplane or ε-tube is constructed that accommodates a maximum number of data points within a defined margin while limiting the deviation from the margin. An example of an ε-tube with slack variables ξ_i is shown in Figure 2.5.

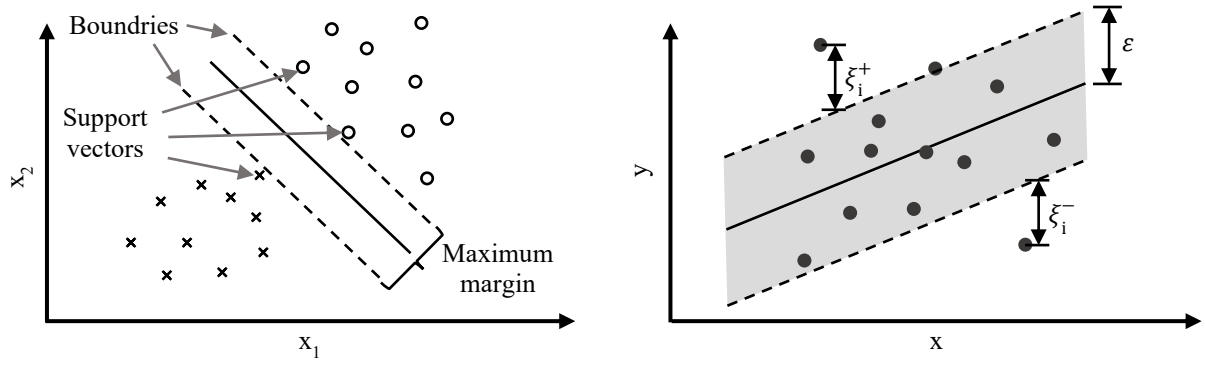

Figure 2.5: Left: Representation of two data classes (circles and crosses) separated by the SVM decision boundaries. Support vectors are depicted for three data points (adapted from GÉRON (2019)). Right: Representation of an ε-tube with data points depicted as circles and two slack variables ξ_i^+ and ξ_i^- (adapted from SMOLA & SCHÖLKOPF (2004)).

Analogously, an optimization problem can be defined, in which points at a distance ξ_i outside the ε-tube are penalized:

$$\min_{w,w_0} \frac{1}{2} \|\boldsymbol{w}^2\| + C \sum_{\mathrm{i}=1}^{\mathrm{m}} \xi_\mathrm{i}^+ + \xi_\mathrm{i}^- \tag{2.26}$$

This problem can also be solved using a Lagrangian dual while accounting for several boundary conditions. (FROCHTE 2019, p. 290)

For both SVM and SVR, a linear decision boundary is predefined. However, data sets are often separated nonlinearly, and linear decision boundaries may not be suitable. For nonlinear separable data sets, a kernel is thus required that provides a function to map the input features to a higher dimensional feature space in which the data is linearly separable. (JOSHI 2020, p. 70) In the higher dimensional feature space, a hyperplane can then be defined to effectively separate the data sets. Frequently used nonlinear kernels are the polynomial kernel and the radial basis function (RBF) kernel. (JOSHI 2020, p. 70-71) Weights for the hyperplane are referred to as hyperparameters. Similar to the weights in linear regression, hyperparameters need to be adapted (tuned) to achieve a generalization of the model and ensure an efficient model performance. Hyperparameter tuning includes various techniques, such as grid search, random search, and gradient-based optimization. (GÉRON 2019, p. 159-161)

Further ML models not part of this work but often used in the literature are decision trees, gaussian process regression, and Bayesian optimization. (JOSHI 2020)

2.2.4 Artificial neural networks

ANNs constitute a class of computational models inspired by the structural and functional attributes of a biological neuron. The perceptron model provides a simple concept of an artificial neuron called a linear threshold unit (GÉRON 2019, p. 281-282). The structure of a perceptron for a linear calculation is provided in Figure 2.6. Each input $x_{\mathrm{j,i}}$ is associated with a weight $w_{\mathrm{j,i}}$ to get a weighted sum of all inputs along a bias b_i. The output y_i of the neuron is then calculated

by applying a nonlinear function $h(z)$, the activation function, to the weighted sum of all inputs: (RUSSELL ET AL. 2010, p. 728)

$$y_{\mathrm{i}} = h\left(\sum_{\mathrm{j=i}}^{N_{\mathrm{i}}} w_{\mathrm{j,i}} x_{\mathrm{j,i}} + b_{\mathrm{i}}\right) \tag{2.27}$$

To account for nonlinear relations, a multi-layer perceptron model can be used, in which perceptrons are connected sequentially and parallel to each other. Figure 2.6 shows a feed forward ANN that is built using multiple perceptrons.

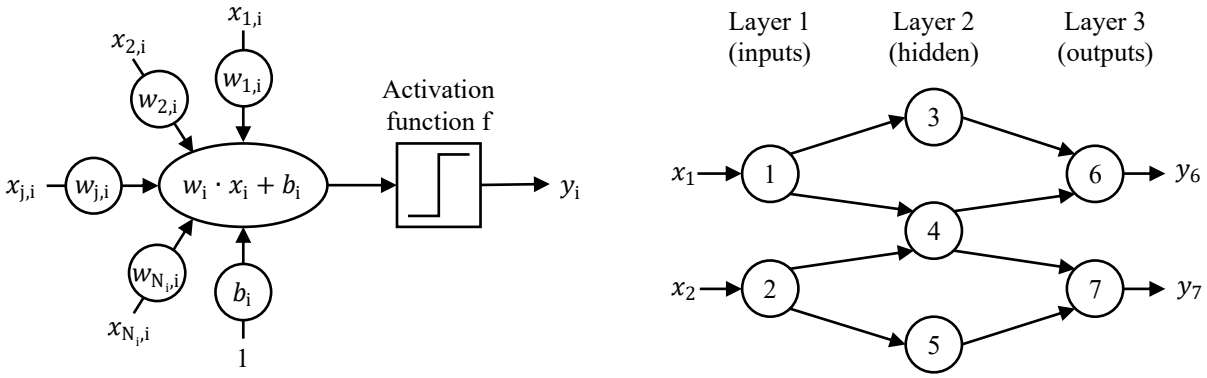

Figure 2.6: Left: Schematic depiction of the perceptron with various inputs and an activation function (adapted from GÉRON (2019)). Right: Representation of feed forward ANN that consists of a multi-layer perceptron with multiple neurons and three layers (adapted from GÉRON (2019)).

The first layer denotes the input layer and the last layer is the output layer. In between, several hidden layers can be implemented, depending on the desired complexity of the model. (GÉRON 2019, p. 286-288) The network is referred to as a fully connected neural network (FCNN) if each neuron is connected to all neurons in the subsequent and previous layer. If multiple output layers are defined, a classification can be performed using the FCNN. (GÉRON 2019, p. 282-283) Different activation functions like the Heaviside step function, the linear function, the logistic function, the hyperbolic tangent function, or the rectified linear unit (ReLU) function can be chosen depending on the task. (GÉRON 2019, p. 288-291)

The application of ANNs requires prior training of the model. An exemplary training process for an ANN is displayed in Figure 2.7. To efficiently train an ANN, a loss function and optimizer are used. During training, weights are iteratively calculated based on the input and target values. The loss function compares the predicted target value to the true target value after each iteration and provides a loss value, which indicates the prediction accuracy. The optimizer updates the weights based on the loss values, and the process is repeated in the so-called backpropagation. (GÉRON 2019, p. 298-299) Frequently used optimizers include algorithms like Adam, AdaMax, or stochastic gradient descent. Furthermore, value normalization is used to normalize heterogeneous data, and regularization methods are applied to reduce overfitting during training. (GÉRON 2019, p. 28-29)

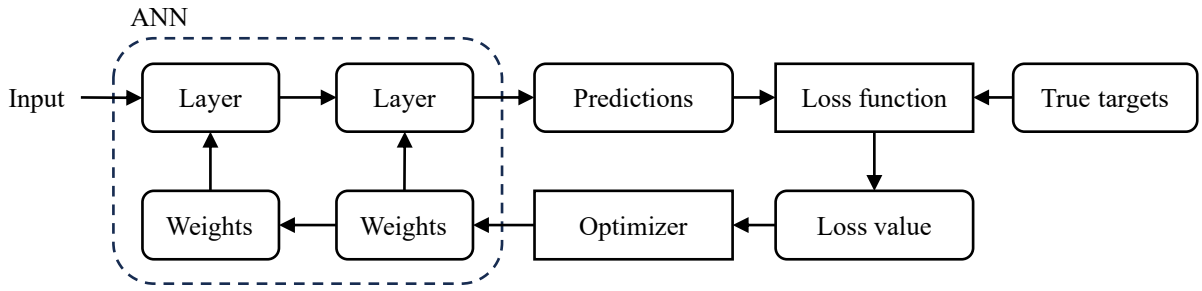

Figure 2.7: Schematic structure of the training process of an ANN, including the loss function and an optimizer that are represented in square boxes (adapted from GÉRON (2019)).

Similar to linear regression and SVR, a generalization of the ANN is desired to achieve a small RMSE for prediction tasks or a high accuracy for classification tasks. Convolutional neural networks and recurrent neural networks represent specialized architectures within the framework of ANNs to handle different data types and tasks (REBALA ET AL. 2019, p. 190). However, these models were not part of this work, and further detailed information regarding ML and ANNs can be found in JOSHI (2020) or GÉRON (2019).

3 State of the Art

In this chapter, the relevant scientific literature for this work is presented and discussed. Three main topics are chosen to be examined in detail and to derive the need for action. Firstly, the impact of the formation process on the cell quality and processing time is assessed in Section 3.1 with an emphasis on fast formation strategies. This includes the choice of electrical parameters and ambient conditions such as temperature and normal stress on the cell. Gas evolution detection techniques targeting the examination of SEI formation are subsequently presented in Section 3.2. A critical aspect in assessing the cell and SEI quality is the identification of the cycle life. Hence, RUL and cycle life prediction approaches using ML are presented in Section 3.3. Based on the evaluation of the state of the art, the research gap and need for action are derived in the final Section 3.4.

3.1 Formation process

The formation process is among the most time-intensive process steps in battery production. WOOD ET AL. (2019) reported a formation time of three to seven days and a high share of floor space within a factory of up to 25 %. During formation, the SEI and CEI are formed by reduction and decomposition reactions of the electrolyte components along with the consumption of Li. In particular, the SEI significantly influences the cell quality (AN ET AL. 2016), and a complete SEI formation is assumed to require multiple charging cycles at currents between C/5 and C/20 (WOOD ET AL. 2015b). This results in high process times and production costs. Hence, several studies aim to implement fast formation strategies and are discussed in the following.

Formation protocols

An early study targeting the reduction of the formation time of LIBs was conducted by LEE ET AL. (2004). The goal was to adapt the formation procedure for cells with a lithium cobalt oxide (LCO) cathode and graphite anode without compromising the cell quality. By evaluating the beginning of the initial intercalation period, a major and a minor SEI formation period were identified. The start of the intercalation period at approximately 0.3 V vs. Li/Li^+ marked the boundary between the two formation phases. Based on the potential range of EC reduction, the major SEI formation period was reported to start at approximately 1.0 V vs. Li/Li^+ (JEONG ET AL. 2001). Different single-cycle formation protocols were then derived with cut-off voltages ranging from 3.6 V to 4.2 V and applied to coin cells as well as cylindrical cells of the type 18650. For the cylindrical cells, a current of C/5 was chosen (except for one deviating cell), and cycle life testing was performed to assess the quality. All configurations with a cut-off voltage greater than 3.7 V did not exhibit a reduced cycle life. An optimum cut-off voltage of 3.7 V was thus concluded, which resulted in a minimum formation time of 4.13 h. This equaled a time

reduction of 69 % compared to a 13.17 h single-cycle reference protocol with a C-rate of C/5. However, only one cell was tested for each of the five configurations. (LEE ET AL. 2004)

AN ET AL. (2017) conducted a study on the fast formation of NMC532/graphite pouch cells by applying a high-potential five-cycle formation protocol. The assumption was that the SEI layer at high SOC is more stable and compact since more lithium is available at the anode (KIM ET AL. 2011). Furthermore, elevated SEI and CEI formation at high SOC was reported due to the occurrence of more reduction as well as oxidation reactions (LU ET AL. 2014). In the experiments, single-layer pouch cells were evaluated with an electrolyte consisting of 1.2 M $LiPF_6$ solved in EC:DEC (3:7). Six different formation protocols were defined with C-rates ranging from C/20 to C/5. The baseline protocols had a lower cut-off voltage of 2.5 V and an upper cut-off voltage of 4.2 V. In contrast, alternative protocols with shallow, intermediate discharge cycles at a lower cut-off voltage of 3.8 V and 3.9 V were proposed. Baseline and alternative protocols were then applied during formation, and the configurations were analyzed in EIS measurements, rate capability testing, and cycle life testing. No significantly diminished cell qualities were obtained for the baseline and alternative protocols. The shortest formation protocol resulted in a formation time of 21 h for a five-cycle high-potential formation protocol with a C-rate of C/5. (AN ET AL. 2017)

In a subsequent study, MAO ET AL. (2018) evaluated five different formation protocols with formation times ranging from 86 h to 10 h. Multi-cycle and single-cycle formation protocols with C-rates ranging from C/10 to C/2 were proposed using NMC811/graphite pouch cells and an electrolyte that consisted of 1.2 M $LiPF_6$ solved in EC:DEC (3:7). A multitude of measurement techniques including post-mortem analysis, rate capability testing, cycle life testing, impedance analysis, and x-ray photoelectron spectroscopy (XPS) analysis were applied to assess the quality. The 10 h formation protocols were reported to exhibit lithium plating and decrease capacity retention. In contrast, the formation protocols with a duration of 26 h and 30 h also exhibited lithium plating but did not have a reduced cycle life. The authors hypothesized that plated lithium can be reactivated if a sufficiently low C-rate is selected during initial cycling. Only the 86 h reference formation procedure did not exhibit lithium plating but showed increased resistance and reduced cycle life compared to the 26 h and 30 h formation protocol. Summarizing, all formation protocols with a C-rate of C/2 during formation exhibited safety-critical lithium plating and were therefore reported to not be suitable to apply in industrial battery production. (MAO ET AL. 2018)

The influence of a constant voltage (CV) step at the upper cut-off voltage during formation was examined by MÜLLER ET AL. (2018). Two three-cycle formation protocols were compared using NMC111/graphite pouch cells and an electrolyte with 1 M $LiPF_6$ as conducting salt, EC:EMC (3:7) as solvents, and 2 wt% VC as well as 2 wt% biphenyl as additives. Both formation protocols used a C-rate of C/2 and a voltage range from 2.7 V to 4.2 V for each cycle. However, one protocol had a CV step with a terminal current of C/50 at the upper cut-off voltage of 4.2 V. The cell quality was examined using cycle life testing and differential voltage analysis (DVA), along with post-mortem analyses. Cells without a CV step displayed an accelerated capacity fade during cycle life testing, and DVA revealed an increased graphite and lithium loss. This

was attributed by the authors to an inhomogeneous and porous SEI. Energy-dispersive X-ray spectra of the cells without the CV phase further revealed an inhomogeneous material composition during post-mortem analysis, supporting the hypothesis of inhomogeneous SEI formation. (MÜLLER ET AL. 2018)

RAGO ET AL. (2019) compared two formation protocols with 13.2 h and 186 h formation time in pouch cells with a Si-Gr anode and NM532 cathode. The reference formation protocol (186 h) consisted of five full cycles at C/20 within a voltage range of 3.0 V and 4.1 V. Similar to AN ET AL. (2017), the fast formation protocol (13.2 h) consisted of several cycles at high voltages above 3.9 V. Cycle life testing and post-mortem analysis using scanning electron microscopy, energy-dispersive X-ray spectroscopy, and XPS indicated a similar cell quality and stable SEI for both formation protocols. However, XPS data revealed different SEI compositions since more LiF was detected in the cells that were subjected to the fast formation protocol. (RAGO ET AL. 2019)

So far, all studies chose conventional CC or constant current, constant voltage (CC-CV) charging and discharging for the formation protocols. A SOC-dependent current profile is frequently deployed during battery cell operation to prevent lithium plating and avoid degradation (KOLETI ET AL. 2021). These profiles can either be chosen based on empirical studies or based on electrochemical models (LEE ET AL. 2022). DREES ET AL. (2021) applied an ECM to adapt the current profile during formation based on the anode potential and to prevent lithium plating. Tracking the anode potential is required to avoid a negative potential, in which lithium plating is likely to occur. The ECM was parametrized using three-electrode laboratory cells, from which fast formation strategies were derived and applied to NMC622/graphite pouch cells. An initial current at a C-rate of 3 C was selected in the fast formation protocol, which was subsequently reduced based on the parametrized ECM. The cells were discharged at 2 C, resulting in an overall formation time of 45 min. The ECM-based approach was compared to four single-cycle fast formation protocols with 1 C CC as well as 1 C CC-CV charging procedures with varying discharging C-rates that resulted in formation times between 141 min and 96 min. The cell quality was assessed using cycle life testing at 1 C, and no significant difference in capacity fade was reported for the various formation protocols. The authors emphasized the need for further research regarding the SEI morphology and local lithium plating. (DREES ET AL. 2021)

In a follow-up study, DREES ET AL. (2023) compared five different formation protocols in three-electrode laboratory cells with NMC622 cathode and graphite anode. A low-current, two-cycle formation protocol served as a reference, which consisted of a first cycle at C/20 and a second cycle at C/5. Similar to AN ET AL. (2017) and RAGO ET AL. (2019), two fast formation protocols with multiple high-voltage cycles between 3.9 V and 4.2 V were designed, which differed in the initial charging rate (0.8 C and 0.2 C). A fourth protocol consisted of the adapted current profile previously reported and an initial current of 1.5 C. The last protocol consisted of a CC-CV charging step with a 1.5 C charging current, a C/20 termination criterion during CV charging, and a discharging current of 1 C. Optical post-mortem analysis revealed lithium plating for the cells charged with the 1.5 C CC-CV formation protocol. For the other strategies, no lithium plating was observed, and only minor variations in the electrochemical performance were

detected. The current-adapted formation protocol resulted in the lowest formation time of 1.68 h and the best capacity retention, particularly at high-temperature storage. However, the fast formation approaches were applied to small laboratory coin cells with reference electrodes only, and a transfer to large-format cells is challenging. (DREES ET AL. 2023)

Ambient temperature and normal stress

The effects of mechanical loads and temperature variations during formation were analyzed by HEIMES ET AL. (2020). A single-cycle CC-CV formation protocol with a (dis)charging C-rate of 1 C was selected. Variations in the temperature (0 °C to 50 °C) and normal stress (0 kN to 1.7 kN) were applied to NMC622/graphite pouch cells. A C-rate of 1 C was chosen since previous experiments by the authors did not show a diminished cycling behavior when compared to a formation protocol with 0.3 C. The temperature was tracked throughout the entire formation, and the capacity after formation was used as a quality indicator. Higher normal stresses of 1.7 kN were found to be beneficial for cell quality and formation time reduction. This was most likely due to a reduced impedance and thus smaller overpotentials. Furthermore, the highest tested temperature of 50 °C in combination with the greatest normal stress of 1.7 kN resulted in a formation time of 170 min. However, no detailed analysis regarding the cycle life was conducted, and no information regarding lithium plating was provided. (HEIMES ET AL. 2020)

YAN ET AL. (2020) evaluated the influence of formation temperature on the cell properties in half-cells and NMC532/graphite coin cells. By analyzing the capacity and impedance during formation and subsequent cycling, a formation temperature of 25 °C was reported to be beneficial for SEI formation. A lower temperature of -10 °C resulted in a low ionic conductivity in the SEI, and a high temperature of 60 °C caused severe side reactions. These hypotheses were not verified by the authors, and information regarding the applied materials and formation protocols was omitted. (YAN ET AL. 2020)

In summary, there are a multitude of influencing factors during formation and studies have reached different conclusions for improved formation protocols. A comprehensive review regarding state of the art and future formation procedures is provided by SCHOMBURG ET AL. (2024).

3.2 Detection of gas evolution

The SEI formation is accompanied by gas evolution due to the decomposition of the electrolyte and reduction reactions (cf. Section 2.1.4). Complete evolution and subsequent gas removal during formation is essential since residual gases lead to a pressure on the housing and a safety hazard during LIB operation (AIKEN ET AL. 2014). Providing insights into the gas evolution is essential to understanding the SEI formation process and further optimizing formation procedures in battery production. Several studies have been conducted that examined the gas composition using differential electrochemical mass spectrometry (DEMS) in custom laboratory cells. In DEMS, an electrochemical system (i.e., a half-cell or full-cell) is connected to a mass spectrometer to analyze the gas composition in real-time. A comprehensive overview of DEMS studies can be found in KIM ET AL. (2023).

Gas composition analysis

An early study regarding the gas evolution during SEI formation was conducted by BUQA ET AL. (2006). Anodes with highly crystalline graphite and two electrolytes based on a mixture of EC:DMC as well as EC:PC were examined. Several gases like H_2, C_2H_4, and C_3H_6 were detected and correlated to the respective half-cell potential. A key result was the detection of exfoliation of the graphite anode in EC:PC-based electrolytes. The introduction of VC caused a pronounced SEI formation before exfoliation, highlighting the relevance of the electrolyte composition and the monitoring of the gas evolution. (BUQA ET AL. 2006)

The morphology of the SEI in dependency of the formation current was studied by MÄRKLE ET AL. (2011) by tracking reaction products during SEI formation. A graphite anode in an EC-based electrolyte and PC-based electrolyte was examined. The results showed that exfoliation could be suppressed in the EC-based electrolyte when a sufficiently high current is applied. For PC-based electrolytes, no favorable effect was detected when using higher currents, indicating the need for precise tuning of the applied current. (MÄRKLE ET AL. 2011)

In a subsequent study, DEMS was further developed to be used in life cycle tests with 20 cycles by adjusting the measurement design and cell layout (BERKES ET AL. 2015). To improve the setup stability, a modified version of DEMS, the online electrochemical mass spectrometry (OEMS), was subsequently developed (TSIOUVARAS ET AL. 2013).

BERNHARD ET AL. (2015) quantified the gas evolution during SEI formation and the impact of residual water by OEMS. OEMS enables the stable analysis of gas composition over multiple cycles. In a water-free electrolyte, C_2H_2 was detected as the main gas during SEI formation. Increasing the water content to 4000 ppm resulted in a substantial evolution of H_2. However, applying a precharge to decrease the anode potential in a VC-containing electrolyte reduced the gas evolution significantly. This resulted in an early SEI formation with a different molecular composition. The study shows that SEI composition substantially influences gas evolution during cycling. (BERNHARD ET AL. 2015a)

Using a similar OEMS setup, SCHWENKE ET AL. (2019) analyzed the effect of VC and FEC during formation on the SEI formation and gas evolution in lithium iron phosphate (LFP)/graphite cells. Both additives were shown to produce mainly CO_2 during formation, which reacted further to form $LiCO_3$ and a stable SEI. Furthermore, CO_2 led to a first passivation layer at approximately 1.5 V vs. Li/Li^+ if water and HF were present. The authors thus conclude that traces of water and CO_2 generation are beneficial for the initial SEI formation. (SCHWENKE ET AL. 2019)

All DEMS and OEMS studies that were presented so far used small laboratory cells to analyze the evolution of gas. To evaluate the gas evolution in industrial-relevant cell formats, MATTINEN ET AL. (2020) developed an OEMS setup capable of analyzing 18650-type cylindrical cells. The setup enabled the continuous evaluation of reaction gases during cycling and revealed a strong C_2H_4 evolution during fast charging. However, a constant argon flow was required to deliver the gases to the mass spectrometer, which caused solvent evaporation in the electrolyte and a potential measurement bias. (MATTINEN ET AL. 2020)

A similar approach of using OEMS to examine large-format plug-in hybrid electric vehicle 2 (PHEV2) cells was introduced by MISIEWICZ ET AL. (2023). An intermittently closed OEMS system was designed by fitting an adapter plate to the lid with an O-ring sealing. The 48 Ah PHEV2 cell contained a NMC811/graphite chemistry, and two formation cycles were performed at a C-rate of C/15. An initial strong evolution of H_2 and C_2H_2 caused by the SEI formation was detected and correlated to the respective cell voltage. At voltages above 4.09 V, significant CO_2 evolution was measured that presumably resulted from cathode lattice collapse and subsequent O_2 release. The O_2 was then reduced to CO_2, and a pressure increase within the cell was detected. (MISIEWICZ ET AL. 2023)

Both OEMS and DEMS provide high sensitivity and are frequently used to examine (electro-) chemical processes within the cell. However, laboratory cell setups are required for the analyses or significant interventions in large-scale cells have to be conducted to extract the gases. Hence, setups were developed for minimally invasive gas extraction and composition analysis.

Gas sampling approaches

SCHMIEGEL ET AL. (2020) introduced a gas sampling port in the gas bag of a pouch cell. A small pipe with a cannula port was incorporated into the gas bag and sealed airtight. The evolved gases are then extractable by a syringe and analyzed in a mass spectrometer. By comparing a regular cell to the modified cell with a sampling port in cycle life testing and DVA, the authors concluded that the sampling port did not influence cell behavior. Furthermore, absolute gas quantities were measured using a setup based on the buoyant force first introduced by AIKEN ET AL. (2014). A validation was conducted by examining the known influence of FEC on CO_2 evolution during formation, and a high concurrence was concluded. (SCHMIEGEL ET AL. 2020)

A similar setup of a pouch cell with a gas sampling port in the gas bag was presented by LEIßING ET AL. (2020). Gas was extracted from the cell using a gastight syringe and sealed cannula. The gases evolved during formation in 5 Ah NMC622/graphite pouch cells were analyzed in gas chromatography with a barrier discharge ionization detector. The results confirmed previous studies in which CO, H_2, and C_2H_2 were detected during SEI formation. (LEIßING ET AL. 2020) However, no evaluation of the influence of the sampling port on the cycling behavior was conducted. Furthermore, no mention or comparison was made with the study by SCHMIEGEL ET AL. (2020), although the same research group published both studies within three weeks.

The direct coupling of a pouch cell to a mass spectrometer using a capillary column was presented by GENG ET AL. (2020). A 115 cm long glass capillary was sealed in the gas bag of the pouch cell to extract the gases. By applying an external pressure of approximately 35 kPa, the gases were pushed into the mass spectrometer during formation without relying on manual extraction or a carrier gas. The setup was validated using a 420 mAh NMC811/graphite pouch cell. Consistent with previous studies, C_2H_4 from EC decomposition was detected as the dominating gas species during SEI formation. Moreover, the oxidation of the electrolyte at high voltages and subsequent CO_2 evolution were presented. (GENG ET AL. 2020)

Gas volume analysis

The presented approaches to detect gas species during formation rely on special laboratory cells or modifications of the cell housing. A different approach to gain insights into the cell-internal processes is the determination of the absolute gas quantity instead of the gas composition.

AIKEN ET AL. (2014) first introduced a measurement setup that utilizes the buoyant force to continuously track the gas evolution. A NMC111/graphite pouch cell was attached to a strain measurement device and injected into an immersion bath filled with mechanical pump oil. If gas is produced during formation, the volume and thus the buoyant force increase, resulting in a change in force at the strain measurement device. The change in force at the strain measurement device is directly proportional to the volume increase with respect to the immersion fluid density. Variations in the formation protocols, electrolyte additives, and clamping were analyzed, and a maximum precision of 4 µL for the measurement setup was reported. An initial substantial gas evolution was measured for all formation protocols, which decreased during the subsequent cycling. This indicates the occurrence of gas-consuming reactions, forming either solid or liquid products. For clamped cells, the gas consumption was reduced, and cells containing VC as an additive showed a decrease in the initial gassing volume. (AIKEN ET AL. 2014)

A further study utilizing the immersion bath is presented by SELF ET AL. (2015). The authors combined mass spectroscopy with the in-situ gas volume measurement to examine the formation of NMC442/graphite pouch cells at different temperatures, charging currents, and VC contents in the electrolyte. A first gassing period at approximately 3.7 V caused by C_2H_4 formation was identified, and a second gassing period at approximately 4.3 V due to CO_2 release. Gas volumes during the first gassing step decreased with increasing VC concentrations, whereas the gas volumes in the second gassing step increased. At higher temperatures, gas formation increased in both gassing periods, indicating a higher reactivity. (SELF ET AL. 2015)

In the combined work of ELDESOKY ET AL. (2021) and ELDESOKY ET AL. (2022), gas evolution during formation and aging was examined for different artificial and natural graphites paired with NMC811. Again, the measurement setup described by AIKEN ET AL. (2014) was utilized. As a result, natural graphite with a high surface area exhibited the worst passivation since substantial gas evolution continued after initial charging and SEI formation. By combing the gas evolution with mass spectroscopy and DVA, a correlation was found between the C_2H_4/CO_2 ratio during formation and the first cycle coulombic efficiency. Furthermore, VC and FEC improved the SEI formation in terms of complete surface passivation and reduced EC consumption. (ELDESOKY ET AL. 2021, ELDESOKY ET AL. 2022)

ALSHEIMER ET AL. (2023) determined the gas evolution in NMC111/LTO pouch cells using a similar immersion bath measurement setup. In the study, the impact of formation temperature on the gas evolution during formation and cyclic aging was evaluated. The formation consisted of three CC-CV cycles at a C-rate of C/10 and a potential range of 1.5 V to 2.8 V, followed by cyclic aging at C/2 at 40 °C. Increased gas evolution at higher temperatures was detected, which was accompanied by stronger evolution of C_2H_4 and CO_2. However, the continuous gas evolution was suppressed during subsequent cycling when a formation temperature of 60 °C was

chosen, and an improved capacity retention was observed. The authors concluded that a higher formation temperature of 60 °C promoted a stable SEI formation and higher initial capacity without compromising the rate capability or cyclic aging. (ALSHEIMER ET AL. 2023)

Several studies examined the gas evolution and composition during SEI formation for different cell chemistries, environmental conditions, and formation procedures. The results indicate that analyzing the gas evolution either by gas composition or quantity enables the observation of cell-internal processes. However, most studies required either specialized laboratory cells (e.g., for OEMS or DEMS) or modifications in the test or cell setup. To transfer the findings from a laboratory environment to an industrial application, scalable approaches are missing. Furthermore, the influence of the gas evolution on essential quality measures like the cycle life is often omitted.

3.3 Cycle life prediction

Determining the SEI quality is often associated with cycle life testing since an inferior SEI might only be detected through a reduced cycle life (WANG ET AL. 2018). This slows the process advancement since cycle life assessment requires several months of testing. Consequently, different approaches to predicting the cycle life or RUL were addressed in the literature. RUL prediction aims to estimate the degradation behavior of a product using data sources and prognostic algorithms (SAHA ET AL. 2009). RUL prediction for LIBs is particularly challenging due to their nonlinear degradation behavior. A turning point is frequently observed that separates the initial linear and subsequent nonlinear degradation behavior. (SCHUSTER ET AL. 2015b) A non-uniform, stochastically distributed degradation behavior was also detected in industrial-manufactured LIBs from a BEV (SCHUSTER ET AL. 2015a). Due to this high significance, multiple studies were conducted to predict the RUL, which were predominantly based on physical or semi-empirical models, as well as data-driven models. A complete listing would exceed the scope of this work, and an excerpt of the most relevant publications is presented in the following.

Semi-empirical and physical models

Semi-empirical models try to model distinct cell properties based on physical or electrochemical interrelationships. In early research, the emphasis was on modeling the SEI growth (CHRISTENSEN & NEWMAN 2004) and lithium deposition (ARORA ET AL. 1999). BLOOM ET AL. (2001) were among the first to semi-empirically model and predict the calendrical and cyclic degradation behavior of lithium nickel cobalt oxide (LNCO)/graphite cells. Sixty 18650-type cylindrical cells were subjected to variations in the temperature, storage time, and SOC. The degradation was then determined based on the power fade as well as impedance increase and predicted using models based on Arrhenius kinetics. A good agreement of experimental to calculated data was reported since a high regression coefficient $r^2 > 0.9$ was present. (BLOOM ET AL. 2001)

By applying a single-particle model, PINSON & BAZANT (2013) could predict the capacity fade in commercial cells with a graphite anode. The model was particularly successful in predicting temperature-dependent degradation using Arrhenius kinetics. The cycle life distribution was

found to be consistent with a Gaussian distribution, however, a linear capacity fade was assumed in the model.

Nonlinear degradation was successfully modeled by YANG ET AL. (2017) based on an electrochemical-thermal model that was capable of predicting SEI growth and lithium plating. The physics-based model was applied to LIBs of a plug-in electric vehicle undergoing moderate cycling at ambient temperature. SEI growth was reported to be predominant during linear aging, whereas lithium plating was attributed to the transition from linear to nonlinear aging. The onset of lithium plating also caused an accelerated SEI formation and a self-amplifying degradation effect. (YANG ET AL. 2017)

Since computational power increased significantly over the last years, models could also be increased in complexity. KIM & LEE (2020) compared three-dimensional (3D) cell models with a lumped cell model with equivalent resistances to predict the degradation behavior of 20 Ah pouch cells. Several sub-domain models were considered in the approach, including material and charge conservation, charge transfer kinetics, as well as degradation mechanisms on a particle, electrode, and cell domain. Both models were able to predict the degradation behavior with high accuracy, whereas the 3D model exhibited the best agreement with an error of less than 1 %. However, run times of 6 days were reported for the 3D model, whereas the lumped cell model required only 35 min of computational time and similar error values. (KIM & LEE 2020)

Physical and semi-empirical models show great potential in predicting the degradation behavior of LIBs. To date, a key challenge remains the computational effort, the complexity of the models, and limitations in covering multiple degradation modes. Comprehensive reviews of physical modeling as well as semi-empirical modeling for degradation and RUL prediction is provided by RENIERS ET AL. (2019) and ELMAHALLAWY ET AL. (2022).

Data-driven prediction

Data-driven approaches to predict the degradation and RUL of LIBs increased in popularity over recent years. The advantage stems from their straightforward implementation, facilitated by the availability of large data sets (e.g., obtained through laboratory cycling or monitoring of BEV cells), thus overcoming the need for complex modeling techniques.

Among the first, NUHIC ET AL. (2013) presented a comprehensive data-driven approach to predict the RUL of LIBs utilizing SVR. The study included data preparation, feature extraction, and model optimization to find optimal hyperparameters. Six automotive cells were examined under different load profiles in a BEV. Eleven driving cycles were used for the training and prediction of capacity fade during seven successive driving cycles. The authors reported high accordance in the RUL, however, no detailed metrics to evaluate the performance were provided. (NUHIC ET AL. 2013)

An alternative approach based on a particle filter method was shown by MIAO ET AL. (2013). A total of four cells, which were not specified in the study, were used to evaluate the model performance. Two scenarios to predict the RUL were compared with 15 and 32 testing cycles as

input data. Including 15 input cycles resulted in a prediction error of approximately 4 %, whereas 32 cycles resulted in an error of less than 2 %. Considering the cycle life of approximately 50 cycles, the training data set included a significant share of the overall cycles. (MIAO ET AL. 2013)

HU ET AL. (2014) applied a Gauss–Hermite particle filter technique for the RUL prediction of LIBs for medical devices. The developed method was verified using four prismatic test cells cycled under laboratory conditions and four prismatic field cells. Cycle life for the test cells ranged from approximately 580 to 700 cycles. RUL prediction of one cell revealed a high similarity of predicted to observed cycle life when more than 200 cycles were used as input data. Again, no prediction metrics for the RUL were quantified in detail. (HU ET AL. 2014)

RUL prediction based on functional principal component analysis and a Bayesian approach was presented by CHENG ET AL. (2015). Four cells from a National Aeronautics and Space Administration (NASA) dataset with cycle lives ranging from approximately 100 to 170 cycles were analyzed using both models. The discharge capacity was used as input data, and a sensitivity analysis was conducted utilizing an increasing number of input cycles. The prediction error decreased from 11 % when 10 input cycles were considered to 6 % with 120 input cycles. Bayes updating as further modeling technique was subsequently included to lower the prediction error to 7 % using 70 input cycles. (CHENG ET AL. 2015)

The NASA dataset was also used by ZHOU ET AL. (2016) for RUL prediction with battery health indicators. A relevance vector machine was introduced to extract the health indicators, which were composed of a series of discharging voltages. To evaluate the performance of the relevance vector machine, health indicators from the first 80 and 100 cycles were used as input. In both cases, the absolute prediction error was less than five cycles. However, more than 50 % of the data set was used as input for the models. (ZHOU ET AL. 2016)

Deep neural networks (DNN) with autoencoder for RUL prediction were examined by REN ET AL. (2018) using the same NASA dataset. 15 features from voltage, current, and temperature data were extracted from the dataset. A sequential feature preparation method was presented that included feature fusion, conversion, and normalization to enable the implementation of a DNN. 20 input cycles were selected, resulting in a prediction accuracy of approximately 93.3 % for the DNN. The results were benchmarked against Bayesian regression, linear regression, and SVM, which exhibited lower prediction accuracies between 88.0 % and 89.4 %. The authors concluded that a nonlinear model is favorable for predicting the RUL. (REN ET AL. 2018)

RUL prediction using ANNs in combination with particle filter algorithms was examined by WU ET AL. (2019). The ANN contained two and three neurons within the hidden layers and a hyperbolic tangent as an activation function. Four LCO/graphite pouch cells alongside the NASA dataset were utilized to evaluate the model performance. For the pouch cells, a MAPE of 46 cycles was achieved using approximately 50 % of the dataset for training. The MAPE was further reduced to 29 cycles and 2 cycles when including approximately 67 % and 83 % for training. For the NASA dataset, results comparable to those of REN ET AL. (2018) were achieved.

SEVERSON ET AL. (2019) performed cycle life prediction and classification using 124 commercial LFP/graphite cylindrical cells of the type 18650. 72 different fast charging strategies were applied, and several metrics such as the cell voltage, current, internal resistance, and cell housing temperature were continuously tracked. Depending on the testing protocol and cell quality, cycle lives ranged from 150 to 2300 cycles. The study aimed to predict the cycle life before capacity degradation occurred. Thus, only data from the first 100 cycles was used for feature extraction and regression analysis. Features were extracted from the charge-voltage curve, temperature, and internal resistance of the cells. Three models based on regularized linear regression were presented that contained different numbers of features. The variance of the discharge capacity as a function of the voltage between the 10^{th} and 100^{th} cycle was identified as the most relevant feature, yielding a mean test error of 11.4 %. The best model achieved a minimum test error of 9.1 % using six features. For classification, two logistic regression models that contained different numbers of features were compared. The task was to classify cells into two groups with low cycle life (< 550 cycles) and high cycle life (≥ 550 cycles) using five cycles as input data. The best classification model with 18 input features achieved an accuracy of 97.5 %. (SEVERSON ET AL. 2019)

ZHU ET AL. (2019) applied different ML models for early cycle life classification using a similar dataset as SEVERSON ET AL. (2019) containing 138 LFP/graphite cells. The aim was to classify the cells into two groups with a threshold at 550 cycles. A total of eight feature sets were compared by extracting individual features from different cycles within the first 100 testing cycles. Discharge capacity difference between the initial two cycles was found to be the most relevant feature. The prediction accuracy was then compared using two feature sets and eight different models: decision tree, k-nearest neighbor, ANN, adaptive boosting, gaussian process regression, random forest, linear SVM, RBF SVM, and Naive Bayes. The classification accuracy varied significantly between the models, and a maximum accuracy of 95.2 % was achieved using decision trees. (ZHU ET AL. 2019) However, the classification accuracy was smaller than previously reported by SEVERSON ET AL. (2019).

A further study with the same data set was conducted by JIANG ET AL. (2021) that aimed to reduce the number of input cycles for cycle life classification. A hierarchical Bayesian model was applied, and data from the initial three cycles was used. Different classification tasks were evaluated, whereby the number of classification groups varied from two to six. The lowest testing error of 6.3 % was gained using five and six classification groups. A model validation was then conducted for 21 NMC/graphite cells, for which a minimum testing error of 10.4 % was reported. Moreover, the feasibility of combining the hierarchical Bayesian model with the linear regression model from SEVERSON ET AL. (2019) was shown. The combined model achieved a minimum test error of 8.8 % for cycle life prediction. (JIANG ET AL. 2021)

In addition to the research presented above, there are many other publications targeting RUL prediction. Frequently, research groups applied different ML approaches to identical data and feature sets. Mentioning all studies would exceed the scope of this work, however, a comprehensive overview regarding model-based techniques, data-driven techniques, and hybrid-based

techniques for RUL prediction, including their data sources, is presented in ANSARI ET AL. (2022).

3.4 Conclusion and research gap

The presented literature, along the fundamentals, serves as the first descriptive study with a focus on the three main research fields addressed in detail in this dissertation. Key findings are critically reflected in the following, and the interrelationships between formation procedures, gas evolution detection, and cycle life prediction are elaborated to identify the research gap.

Several studies examined formation procedures in industry-oriented cell formats and their impact on the processing time and quality of the LIBs (cf. Section 3.1). The procedures were selected by estimating critical voltage ranges or avoiding lithium plating by controlling the anode potential. However, most approaches focused on adapting current and voltage ranges without providing insights into the cell-internal processes, such as SEI formation. This results in uncertainties regarding the LIBs' quality, as an inferior SEI diminishes the cycle life. Consequently, time-intensive cycle life testing over several months was required in almost all presented studies for a first quality assurance (cf. Section 2.1.5).

Tailoring formation procedures based on the SEI formation is currently challenging in non-laboratory cells since the SEI is only a few nanometers thick, and no inline detection methods are available. However, indirect tracking of SEI formation is feasible by observing gas evolution during formation. Various gases are generated during SEI formation, as well as other side reactions within the LIB. By evaluating the potential ranges during gas evolution, insights into the cell-internal processes are possible. Several studies analyzed the gas evolution and composition during SEI formation in a laboratory environment or small pouch cells with specialized laboratory cells (cf. Section 3.2). Enabling a non-invasive and inline tracking of gas evolution is a highly promising approach for the foundation of SEI-dependent formation procedures. Critical potential ranges during SEI formation are then detectable using the gas evolution measurement, and a termination criterion can be set. Furthermore, the gas evolution provides an additional quality criterion since contaminations, such as elevated water contents, are detectable in the gas evolution.

When modifying production procedures, comprehensive quality assurance is required in battery production. Especially during the initial process design, multiple parameter variations are conducted and evaluated. This requires thorough quality assurance since slight variations during production result in strong variations in quality parameters leading to a reduced cycle life. As a result, time- and resource-intensive cycle life testing is conducted, which causes high costs and inhibits the process development. As described in Section 2.1.4, formation is particularly critical in this regard since quality assurance is only possible indirectly, and the cycle life needs to be evaluated. Recently, multiple data-driven methods were proposed to predict the RUL of a LIB (cf. Section 3.3). All reported studies target the prediction during operation or testing of LIB cells without providing any information on their production processes. Moreover, approaches have yet to be employed to expedite process advancement in production and guarantee

cell quality when modifying formation procedures. To address these issues, a data-driven cycle life prediction approach based on production data needs to be developed and validated.

Examining the state of the art unveiled deficiencies in the design of formation procedures, notably in the inconsistent application of methods to track the crucial cell-internal processes such as SEI formation or gas evolution. Additionally, if approaches were applied, they relied on time-intensive and costly assurance of the cell quality using conventional cycle life testing, which inhibits the process development and optimization. This dissertation addresses this research gap by adapting formation procedures based on gas evolution and by enabling data-driven analysis methods for quality assurance. The overarching aim is to expedite and secure process development in cell finalization, thereby advancing efficiency and reliability in battery research.

4 Research Findings

This chapter presents the research findings elaborated within this work. First, scientific objectives (SOs) are derived in Section 4.1, which constitute the foundation of the dissertation. An overview of the five publications and their allocation to the different SOs is provided in Section 4.2. The key results are then addressed and summarized in Section 4.3, including the contributions made by the co-authors. Section 4.4 concludes with a discussion of the main findings that involves the contribution to the state of the art and a critical reflection.

4.1 Scientific objectives

The SOs are based on the overall objective presented in Section 1.2 and the research gap elaborated in Section 3.4. By addressing the individual SOs in dedicated publications, the fulfillment of the overall research goal is targeted. A total of four SOs are defined:

SO1: Production concept

Initially, a production concept has to be established to allow for the comprehensive tracking of quality-determining product and process parameters in cell finalization. This tracking is essential for associating gas evolution with the formation progress, thus providing the foundation for systematically optimizing the formation process. Furthermore, real-time analysis of quality parameters in a cyber-physical system (CPS) must be facilitated to utilize data-driven approaches for quality assessment.

SO2: Product and process analysis

The identification of the product and process relationships during formation requires the analysis of cell-internal processes. A device for the operando gassing analysis must therefore be developed and validated to enable the precise and non-invasive detection of gas evolution during SEI formation.

SO3: Quality prediction

A methodology for early cycle life prediction is required to rapidly assess the cell quality. For this purpose, a data mining procedure that includes the data and feature selection, modeling, and evaluation must be established. Furthermore, different ML model approaches have to be elaborated and compared in terms of their suitability and application potential.

SO4: Process advancement

The acceleration of process development in cell finalization requires the targeted optimization of formation protocols and immediate quality assurance. The optimization is facilitated

by tracking the SEI formation using operando gassing analysis. To avoid time-intensive cycle life testing, an early cycle life prediction approach has to be implemented to accelerate quality assurance. The goal is to reduce the formation time without impeding the overall cell quality.

The presented SOs aim to establish data-driven analysis methods in the cell finalization of LIB production. Hereafter, each SO is addressed in at least one publication, and the findings are evaluated in the discussion in Section 4.4.

4.2 Overview of the publications

This dissertation includes five scientific publications (P), which are allocated to the individual SOs in Figure 4.1. The publications contain the main findings of the comprehensive prescriptive study and are summarized in Section 4.3.

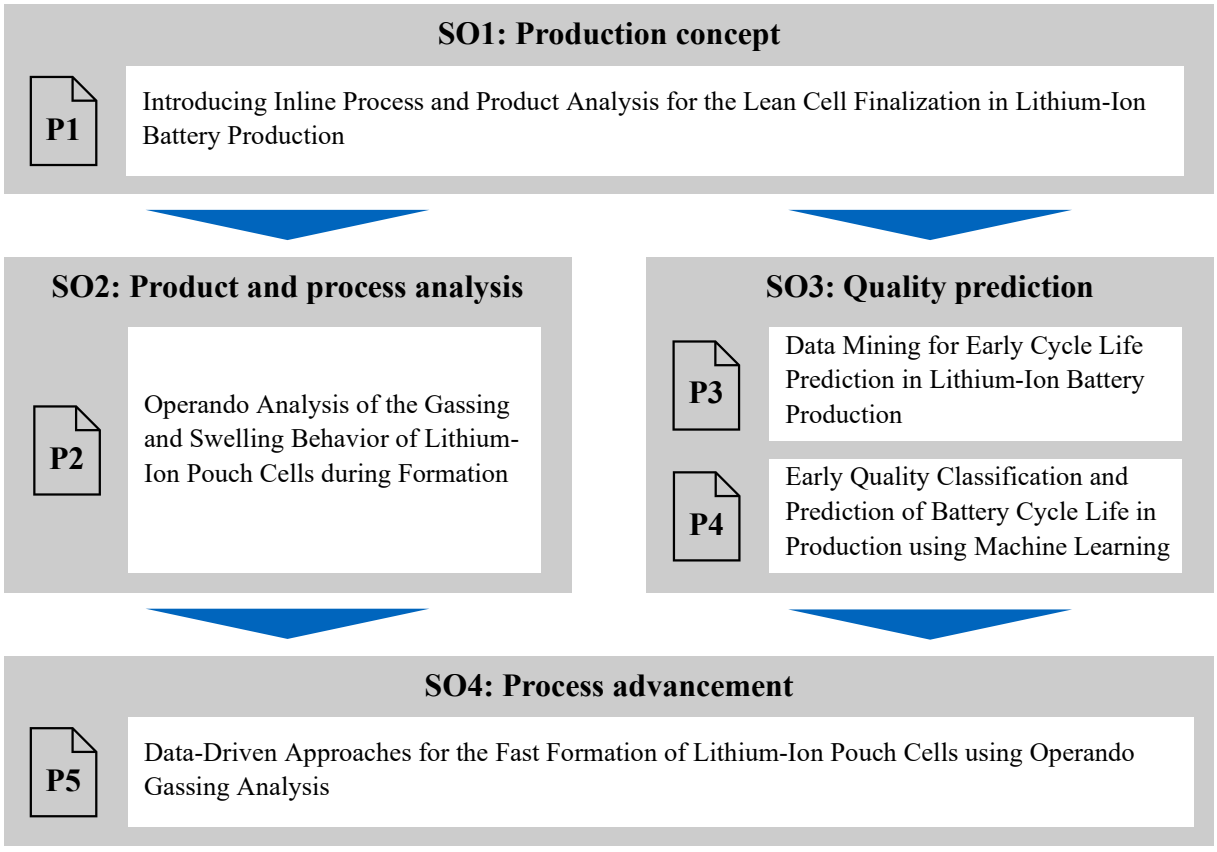

Figure 4.1: Assignment of the individual publications to the SOs within the framework of this dissertation. The blue arrows indicate the knowledge transfer between the SOs.

A production concept for comprehensive tracking of quality-determining product and process parameters is described in P1. This concept serves as a foundation for the interdependency analysis during formation as well as the quality prediction based on production and early cycling data. P2 introduces a novel method to track the gas evolution and cell expansion of LIBs non-invasively during the formation to provide insights into the cell-internal processes. The development of data-driven approaches for early cycle life predictions is addressed in two publications. In P3, a methodology is introduced for efficient data mining in cell finalization and

cycling to predict the cycle life of a LIB at an early stage. Different modeling approaches for classifying and predicting battery cycle life using various data sets are subsequently developed in P4. Finally, the different approaches and methods are combined and validated in P5. In this final study, formation procedures are advanced based on inline gassing analysis, and the developed data-driven methods are employed for early quality assurance.

4.3 Cumulative presentation of the embedded publications

This section provides the overview of publications embedded in the cumulative dissertation. The main findings of each publication are summarized, and the contributions of the authors are clarified.

4.3.1 P1: Introducing Inline Process and Product Analysis for the Lean Cell Finalization in Lithium-Ion Battery Production

The first publication of this dissertation addresses a holistic production concept for the lean cell finalization. First, a literature-based overview of relevant inline measurement parameters during individual steps of cell finalization is presented, such as the ambient temperature, ambient pressure, cell surface temperature, cell weight, impedance, gas composition, water content, and mechanical load. The focus of this study was on the quality-influencing process steps of cell finalization, starting with post-drying and ending with cell degassing. Aging, EOL testing, and grading were not regarded in detail since these process steps pose fewer challenges for the production equipment.

Two innovation modules (IMs) were designed and established based on the identified process requirements and measurement techniques. The IMs comprise multiple process steps with the aim of implementing a lean production approach, which includes the reduction of over-processing, excess transportation, waiting times, and the number of sensors. IM1 combines the process steps of final drying, electrolyte filling, and degassing in a single module, resulting in the mutual use of plant components and sensors. The central element is a circular conveyor plate with individual cell brackets to iteratively fill pouch cells. Multiple filling steps with intermediate soaking times are feasible in the module. IM2 merges the process steps of wetting and formation using a formation rack in a temperature-controlled environment. After placing the cells in the formation rack, the wetting progress is monitored using EIS, and the impedance change is analyzed. A mechanical load is applied to the cell, and the formation is initiated as soon as a sufficient wetting degree is achieved. Furthermore, a cell-specific formation concept based on real-time sensor data is proposed to avoid over-processing and reduce non-value-adding process time.

Both IMs are connected to a virtual production system to evaluate the equipment and sensor data in real-time, thus creating a CPS in which the operation is monitored and controlled. Hence, the determination of the intermediate product state and quality grading is enabled. Features can be extracted from the measurement data, and quality prediction can be performed using a data mining approach in the CPS. Each cell is classified into a quality grade depending on the input

data and processing history. Cells of inferior quality are thus detectable at an early stage, and an adaptation within the process flow at a single cell level is possible. Consequently, defective cells can be removed at an early stage, and processing times can be adjusted. To summarize, the IMs, in combination with a CPS, enable continuous tracking of the product and process parameters in a holistic production concept, as well as the implementation of data-driven approaches for quality assessment during cell finalization.

Author contributions

Sandro Stock proposed the production system for the lean cell finalization and developed, coordinated, and validated the IMs as well as the CPS. Amedeo Ceruti designed the IMs using the computer-aided design software SolidWorks. Florian Günter supported the development of the production concept and the CPS. The manuscript was written by Sandro Stock and edited by Amedeo Ceruti, Floran Günter, and Gunther Reinhart. All authors commented on the results.

4.3.2 P2: Operando Analysis of the Gassing and Swelling Behavior of Lithium-Ion Pouch Cells during Formation

A novel method to evaluate the gassing and swelling behavior of lithium-ion pouch cells is developed in P2 of this dissertation. The aim was to precisely track the gas evolution during formation to elucidate cell-internal processes, such as the SEI formation. A cell expansion bracket (CEB) was designed to connect the cell to the battery tester and individually track the cell expansion and gas evolution using dilatometry measurements. The cell was placed on a base plate, and two aluminum plates (a cell stack plate and a gas bag plate) were located on the gas bag and cell stack. The movement direction of both plates was fixed to one dimension, and their displacement was tracked using contact distance sensors with a resolution of 0.1 µm. Using calibration measurements to account for different sizes of gas bags, a direct correlation between the displacement of the gas bag plate and the volume inside the gas bag was feasible with a volume resolution of approximately 0.6 µl.

To validate the CEB, two cell chemistries were evaluated, and a comparison was made with the established immersion bath measurement setup. The first cell chemistry consisted of a NMC622 cathode, a graphite anode, and a LP572-type electrolyte with 1 M $LiPF_6$ dissolved in EC and EMC with a mass ratio of 3:7 including 2 wt% VC as additive. For the second cell chemistry, a NCA cathode and a Si-Gr anode with a silicon content of approximately 70 % were used. The electrolyte consisted of 1 M $LiPF_6$ dissolved in FEC and DEC with a mass ratio of 1:4. For both cell chemistries, a good agreement of the immersion bath measurement and the CEB was detected.

During the formation, a seven times higher gas evolution for the NCA/Si-Gr cells was detected compared to the NMC/graphite cells. The gas evolution persisted over ten successive cycles for the NCA/Si-Gr cells, indicating continuous gaseous reactions. This effect was attributed to a continuous SEI formation since silicon expands strongly, leading to cracking and reformation of the SEI upon cycling. For the NMC/graphite cells, gas evolution terminated upon reaching 3.6 V in the first charging cycle. Subsequent formation cycling resulted in a continuous decline

in gas volume, indicating ongoing reactions of the gas components to form liquid or solid products. Accordingly, an ideal degassing time could be derived, and formation procedures can be adapted to the real-time gassing behavior.

The CEB enables the precise detection of the gas evolution during SEI formation without cell interference since no specialized cell types or cell modifications are required. This allows for the rapid and easy screening of the cell-internal processes during formation and enables the tailoring of a gassing-dependent formation.

Author contributions

Sandro Stock developed the approach for the operando gassing and swelling analysis and performed the investigation, data curation, and formal analysis. Furthermore, he visualized as well as interpreted the measurement data and prepared the original manuscript. Felix Diller designed the CEB and supported the investigations. Jonas Böhm further developed the CEB and generated the calibration curves as well as the conversion algorithm. Jan Hagemeister aided in the production of NMC/graphite cells and the formal analysis. Alessandro Sommer provided the NCA/Si-Gr cells for the experiments and conducted the electrode manufacturing as well as cell assembly. Rüdiger Daub supervised the research project and aided in the study design. All authors reviewed the manuscript and commented on the obtained results.

4.3.3 P3: Data Mining for Early Cycle Life Prediction in Lithium-Ion Battery Production

In publication P3, a comprehensive data mining methodology for the early cycle life prediction of LIBs was developed. As a general framework, the CRISP-DM approach for data mining was adopted and further developed to be applied in battery production and testing. Each step within the CRISP-DM was elaborated, and a transferable use case was provided. First, a methodology for early cycle life prediction was identified that can be implemented in battery production and development. A total of 29 pouch cells with NMC111 cathode, graphite anode, and LP572 electrolyte were evaluated and served as a data source.

A total of 65 features were extracted from the formation data and the first 20 cycles of cycle life testing. Since the mean cycle life was approximately 250 cycles, less than 8 % of cycle life data was used. Features extracted from the charge-voltage curves served as the first feature source, which included absolute charge and discharge capacities, capacity differences between cycles, and capacity losses. Moreover, the variance, kurtosis, and skewness of the charge-voltage curves were analyzed. The second feature source originated from an incremental capacity analysis (ICA). An optimization algorithm was developed to extract the peak position and heights using a single smoothing parameter. This reduces the bias when performing the ICA, as peak characteristics are sensitive to fluctuations in the charge-voltage curves. Besides the individual peak properties, further central momentums were extracted from the ICA analysis and used as input features.

Three different feature selection techniques were subsequently evaluated and compared in terms of prediction accuracy. Filter methods based on either Pearson’s correlation coefficient

(PCC) or the mutual information (MI) provided the best results when compared to the recursive feature elimination in SVR analysis. A minimum test error of 14.4 % was achieved for SVR with a linear kernel using MI and ten features. Utilizing a RBF kernel and SVR, the minimum test error decreased to 12.6 % when PCC and 19 features were selected.

Finally, a sensitivity analysis for regression as well as classification tasks was performed regarding the impact of the number of input cycles. The best SVR model achieved a mean minimum test error of 8.8 % when 31 input cycles were used. SVM models were used for classification into two groups, whereas the threshold was set at the mean cycle life of 250 cycles. A mean test accuracy of 96.6 % was reached using 23 input cycles. Consequently, only one cell was wrongly classified, indicating the great potential of data-driven models to effectively predict the cycle life at an early stage.

Author contributions

Sandro Stock initially proposed early cycle life prediction using data from the cell finalization and cycling. Furthermore, he developed the methodology, performed the formal analysis, and created the original manuscript. Mahmoud Ahmed created the Python code for feature extraction as well as modeling and developed the algorithm for peak identification in the ICA. Fabian Konwitschny supported the conceptualization and formal analysis. Rüdiger Daub supervised the research project and ensured its funding. All authors edited the manuscript and commented on the results.

4.3.4 P4: Early Quality Classification and Prediction of Battery Cycle Life in Production using Machine Learning

In P4 of this dissertation, data-driven ML approaches were developed for early quality classification and prediction of battery cycle life. The study aimed to compare linear models to ANNs by performing sensitivity analyses and to evaluate the potential of ANNs for quality grading in battery production. Similar to P3, 29 NMC111/graphite cells were used as a data source for the study. Additionally, impedance data from electrolyte wetting was included alongside formation and cycling data. In total, 29 features were selected for the study and listed according to their correlation with the cycle life. The capacity loss and variance in discharge capacity showed the highest PCC of approximately -0.9.

For comparing linear regression to ANNs, a study regarding suitable network architectures was initially conducted. Five different networks were created and evaluated regarding the convergence of the loss function over multiple epochs. The favorable ANN consisted of five hidden layers with neuron numbers ranging from 40 to 8, AdaMax as an optimizer, ReLU as an activation function, early stopping as a regularization method, and an adaptive learning rate that started at 0.1.

Linear regression and the favorable ANN were subsequently compared in a regression task utilizing different feature numbers ranging from 1 to 29 features. In all studies, the ANN achieved lower mean test errors, whereas the advantage differed from 0.5 % when three features were used to 5.2 % when nine features were provided. The lowest test error of 14.3 % for linear

regression was achieved with three features. For the ANN, a minimum test error of 10.1 % was reachable when all 29 features were included. A sensitivity analysis on the number of input cycles from cycle life testing further revealed a slightly better performance of the ANN. However, strongly increased computational power was required for the ANN.

Subsequently, a classification study in two groups using the ANN was conducted, in which the data sources were varied. The classification threshold was set at the mean cycle life of 250 cycles. Initially, only wetting data was used as input for the ANN, resulting in a classification accuracy of 80 %. Adding the formation features improved the accuracy to 88 %. If features from the first 20 cycles of cycle life testing were added, the accuracy improved significantly to 97 %.

Finally, quality grading was elaborated by defining four quality grades with thresholds at 200, 300, and 400 cycles. Exclusively using formation data resulted in an inaccurate grading for cells with a moderate and high cycle life. However, inferior cells with a cycle life below 200 cycles were reliably detected. Including cycling data improved the grading significantly, and only cells with cycle lives close to the grading thresholds were misclassified.

In summary, the data-driven ML approaches showed great potential for identifying defective cells at an early stage. Since defective cells were detectable with production data only, potential process errors and quality deviations can be detected immediately. Thus, cycle life prediction was enabled to serve as a quality assurance measure during cell finalization, and quality assessment is accelerated as efforts for complete cycle life testing are omitted.

Author contributions

Sandro Stock had the initial idea of early cycle life classification and prediction using data from cell finalization and cycling. Furthermore, he developed the methodology, performed the formal analysis, and created the original manuscript. Sebastian Pohlmann created the Python code for feature extraction as well as modeling and supported in the visualization. Florian J. Günter created the original data set and aided in the conceptualization. Lucas Hille and Jan Hagemeister supported in the formal analysis and investigations. Gunther Reinhart supervised the research project and ensured its funding. All authors edited the manuscript and commented on the results.

4.3.5 P5: Data-Driven Approaches for the Fast Formation of Lithium-Ion Pouch Cells using Operando Gassing Analysis

Data-driven approaches for the fast formation of LIBs are presented in P5 of this dissertation. A novel approach was developed to adapt formation protocols based on the operando gas evolution. In the approach, the CEB presented in P2 was used to analyze the gassing behavior during formation for NMC622/graphite pouch cells containing a LP572 electrolyte.

First, single-layer pouch cells (SLPs) with a gold-wire reference electrode (GWRE) were built and formed using a stepwise anode half-cell potential controlled formation procedure. The GWRE is required to independently track the anode and cathode potentials. In the procedure, SLPs are charged in steps of 200 mV, with respect to the anode potential, and discharged to

1.81 V vs. Li/Li^+ upon each partial discharge to reach blocking conditions. Blocking conditions were experimentally determined by the stepwise discharging of a SLP with iterative EIS measurements and evaluation of the charge transfer resistance. All subsequent EIS measurements were performed in blocking conditions to enable the evaluation of the impedance change attributed to the SEI formation. A transmission line model was therefore fitted to the impedance data to extract the SEI resistance. Simultaneously, the gas evolution was tracked using the CEB and correlated with the SEI resistance change. The results showed an excellent agreement between both measurements. Gas evolution and resistance change started at 1.0 V vs. Li/Li^+ (approximately 2.6 V full cell potential) and continued concurrently until 0.6 V vs. Li/Li^+ (approximately 3.0 V full cell potential). The gas evolution then remained constant, whereas the SEI resistance continued to increase until 0.4 V vs. Li/Li^+ (approximately 3.25 V full cell potential), indicating structural changes in the SEI without gaseous reduction reactions.

Having shown the consistency of gas evolution and SEI formation, reference multi-layer pouch cells were examined to identify the gassing period using a three-cycle CC-CV formation protocol and a C-rate of C/10. Gas evolution exclusively occurred during the first charging cycle until a voltage of approximately 3.46 V, afterward, the total gas quantity declined. Consequently, two alternative formation protocols that had adaptations in the applied current (current variation) and voltage range (voltage variation) were derived. The formation time was reduced from initially 55 h to 5.3 h for the current variation and to 2.4 h for the voltage variation.

For quality assurance, a comprehensive EOL test was performed that included aging, capacity checks as well as EIS and DC-IR measurements. In comparison with the reference, both formation variations exhibited slightly smaller initial cell capacities, ranging between 1 % and 1.5 %. These differences might have resulted from the adapted formation protocols or storage times but equalized after a few cycles in the cycle life test. Except for the slightly decreased cell capacities, no significant deviations in the quality parameters were detected for the cells with adapted formation protocols. To assure the cycle life of the cells with adapted formation protocols, cycle life prediction was performed as introduced in P3 and P4. A SVR model was trained using reference cell features from the formation, EOL test, and early cycling data of the first 50 cycles. The SVR model predicted a cycle life of less than 550 cycles for all cells of the current variation and a cycle life greater than 650 cycles for four out of five cells of the voltage variation. Subsequent cycle life testing indeed revealed a lower mean cycle life of 508 cycles for the cells from the current variation compared to 572 cycles for the reference cells. The cells from the voltage variation showed an increased mean cycle life of 612 cycles. This indicates that the current variation formation protocol with a C-rate of C/2 above 3.55 V might deteriorate the cell quality. Overall, a mean test error of 7.4 % was achieved, showing the great potential of data-driven models to predict the cycle life. In addition, observation time during cycle life testing could be reduced by a factor of 10, thus enabling a rapid evaluation of overall cell quality and accelerated process development.

Author contributions

Sandro Stock developed the data-driven approaches and conducted the conceptualization, investigations, data curation, visualization, and original writing of the manuscript. Jonas Böhm

established the building procedure for SLPs with GWRE and evaluated the impedance data. Manuel Ank designed the EOL and cycle life testing procedure. Philipp Rath supported in the manufacturing of the MLPs. Markus Lienkamp and Rüdiger Daub supervised the research project and ensured its funding. All authors edited the manuscript and commented on the results.

4.4 Discussion of the findings

The main findings within the individual publications and the fulfillment of the SOs are addressed below. First, the novelty of the results and their contribution to the state of the art are evaluated in Section 4.4.1. The results and insights are subsequently critically reflected in Section 4.4.2, and areas for further research are identified.

4.4.1 Novelty and contribution to the state of the art

To examine the novelty of this work and its significance in bridging the research gap, a evaluation of the findings in respect to the SOs and the state of the art is conducted. A separation is made into three main categories: data-driven production concepts, data-driven quality prediction, and data-driven process advancement.

Data-driven production concepts

Enabling a production concept for tracking product and process parameters in a CPS was the goal of SO1. In P1, requirements were identified, and a novel production concept with two IMs was presented. The IMs provide detailed instructions for facilitating a convenient and efficient tracking of quality-determining processes and product parameters. Furthermore, a flexible and customizable design was proposed that can be easily adapted for production equipment and small pilot-scale production lines. Considering lean production aspects poses another novelty for cell finalization that has not been addressed previously. Based on the IMs, a virtual production system was introduced to establish a CPS. The CPS enables a real-time quality assessment that provides several improvement potentials. First, a consistent determination of the intermediate product quality is possible by evaluating equipment and sensor parameters. These parameters can then serve as feature sources for a data-driven approach to predict the cell quality at the individual production stages. Finally, an adaptation of the process flow based either on direct parameter analysis or quality prediction is feasible that offers the possibility to control the process flow down to a single cell level. This can lead to several benefits, like the reduction of processing time to the value-adding part only and a process adaptation based on cell-specific quality metrics. The production concept builds the baseline for the subsequent analyses in SO2 and SO3. Consequently, the SO1 is successfully achieved.

Formation is a crucial process in cell finalization and strongly influences overall cell quality (WOOD ET AL. 2019). However, high formation times arise due to the lack of knowledge regarding the SEI formation progress (cf. Section 3.1). To reveal cell internal processes during formation, such as gas evolution during SEI formation, a novel measurement approach (i.e., the CEB) was developed in P2. As concluded in Section 3.2, existing techniques for evaluating the gas evolution relied either on special setups (e.g., immersion bath or DEMS) or modifications

on the cell housing (e.g., gas sampling ports or OEMS). The CEB enabled the precise and inline detection of gas volume in the gas bag and the expansion of the cell stack without modifying the cell or testing conditions. Thus, a realistic and non-invasive examination of the formation procedure was enabled. A disadvantage of the CEB compared to the immersion bath measurement is the initial determination of gassing since only gases within the gas bag can be measured, and dead volumes in the cell stack are not detectable. However, if the void volumes have been filled, the CEB provided a more stable and more precise measurement of gas evolution. Resolutions in the range of 1 µl were feasible using the CEB, and the relatively simple measurement technique allows for an easy multiplication and scaling of the device. Hence, an application in the initial process design in a pilot or scaled production of lithium-ion pouch cells is feasible. The CEB thus enables the detection of cell-internal processes during formation, and the SO2 is fulfilled.

Data-driven quality prediction

A major challenge during LIB production and development is the assurance of cell quality (KWADE ET AL. 2018). While metrics like capacity, resistance, or energy can be checked immediately, cycle life determination requires several months of testing (SEVERSON ET AL. 2019). Thus, several approaches were examined in the literature to determine the RUL using testing data (cf. Section 3.3). In P3, a novel methodology was introduced that exceeds the existing approaches by utilizing data from cell finalization. Adding formation data enhances the data basis and enables an earlier prediction compared to the state of the art. Furthermore, features from ICA were included to provide information on the electrochemical properties during Li^+ intercalation and deintercalation to the prediction models. A simple and transferable algorithm was developed to find the optimum smoothing parameters for the ICA peaks in a reproducible manner. Additionally, different feature selection methods were evaluated in the methodology, and a sensitivity analysis was conducted. P4 enhances the methodology by comparing linear regression to ANNs and by evaluating different feature sources. This was the first study (to the best of the authors knowledge) to exclusively use and combine data sources from cell finalization to classify cells into quality groups according to the predicted cycle life. The utilization of data from cell finalization was shown to be sufficient for the prediction, which enables an easy transferability of the methodology since electrical data from formation, aging, or EOL testing is already provided during manufacturing, and no additional sensors are necessary. Different approaches within the literature aim for a complete digitalization of the production chain, which could enable a quality prediction using the intermediate product data (SCHNELL & REINHART 2016). However, no comprehensive approach to predicting the cycle life has been proposed so far.

Data-driven cycle life prediction using data from cell finalization allows for easy transferability. Furthermore, several benefits for the manufacturer as well as the customer can be obtained. Firstly, early cycle life prediction can enhance the conventional quality assurance process based on isolated metrics such as cell capacity, internal resistance, or self-discharge. Defective cells with a reduced cycle life could be detected at an earlier stage (before aging and EOL test) and subsequently removed, which increases the throughput by creating free production capacity.

Moreover, the time-intensive aging process, which targets the detection of micro short circuits that may result in a reduced cycle life, might be replaced or shortened using the cycle life prediction approach. This is a significant lever for cost savings since formation and aging account for approximately 32.6 % of manufacturing costs and 29.4 % of energy costs (LIU ET AL. 2021). Furthermore, it was shown in P2 that process deviations (e.g., a varying electrolyte quantity) can be identified using cycle life prediction. Hence, processing errors can be identified and corrected at an early stage to reduce scrap. The cycle life prediction hereby serves as a quality gate to ensure high product quality and manufacturing stability.

Finally, the manufacturers can provide their customers with an estimate of the cycle life (under defined cycling conditions) as an additional quality parameter. The predicted cycle life can either be provided as an absolute value or a cycle life range can be assigned, similar to the overall quality grading at the end of the production. Consequently, improved grading is achievable, and quality grades can be chosen depending on the predicted cycle life. This way, inferior cells might be used in applications that do not require a maximum cycle life, and scrap as well as costs can be reduced. These benefits indicate the great potential for data-driven quality prediction during cell finalization, and the SO3 is fulfilled.

Data-driven process advancement

Several studies have been conducted to optimize formation protocols by varying the current or voltage profiles (SCHOMBURG ET AL. 2024). These approaches were either based on assumptions regarding the voltage ranges for SEI formation or the determination of maximum current profiles to avoid lithium plating (DREES ET AL. 2023). However, information on the cell-internal processes, such as SEI or gas formation, was not included in the approaches, resulting in uncertainty regarding the overall LIB quality. Quality was then assured using cycle life testing over multiple months (cf. Section 3.1). This results in time-intensive process development cycles. In P5, a novel method was introduced to design formation protocols and concurrently assure cell quality. The method was based on the production-oriented idea that formation is considered complete when the SEI is sufficiently formed, and gas evolution is completed to allow for subsequent degassing. Formation protocols were adapted using the CEB that was developed in SO2 and implemented in the CPS from SO1 to track the gas evolution in real-time. Thus, a single measurement was sufficient to determine critical voltage ranges during gaseous SEI formation. The foundation for coupling gas evolution and SEI formation was supported by using a stepwise formation protocol to track the SEI resistance increase and gas evolution simultaneously utilizing the CEB. For this, a SLP setup with GWRE was proposed that allows for a precise analysis of the SEI formation on the anode using potentiostatic EIS. This also provides a novelty since GWREs were so far primarily utilized on a coin cell basis, which is limited in providing information for large-scale cell formats.

Subsequently, formation protocols were adapted, and the quality was immediately assessed using a comprehensive EOL test and cycle life prediction. The cycle life prediction approach from SO3 based on cell finalization data was thus utilized. For both formation protocol adaptations, a different cycle life prediction range occurred, indicating a quality deviation that was not detectable in the EOL test. Subsequent cycle life testing revealed a difference of approximately

140 cycles for the mean cycle life between both adaptations. This shows the great potential of cycle life prediction for early quality assurance. Less than 10 % of overall testing time was required for the prediction, resulting in accelerated development cycles. The approach is particularly useful in the early phase of development and scale-up since multiple material combinations need to be screened, and processing times have to be defined to achieve the targeted output of the factory. These findings enable data-driven process advancement and mark the successful fulfillment of SO4.

4.4.2 Critical reflection

All studies within this dissertation were conducted at the *iwb* pilot production line with semi-automatic production equipment. Therefore, the production concepts presented in P1 are solely in part transferable to a high-throughput industrial scale. Although the design was largely adopted on a pilot scale at the *iwb*, a further scale-up cannot be automatically assumed. The IMs should thus be regarded as functional concepts to introduce a CPS without specific design prescriptions. The conceptional idea of intermediate quality assessment using a CPS to provide quality gates is applied in various industries. However, the proposed single-piece flow with cell-specific processing constitutes a novel idea in battery production that should be examined in further studies.

The production line at the *iwb* is limited to the manufacturing of pouch cells. Thus, all studies were based on results from pouch cell analyses. The CEB developed in P2 is solely applicable to pouch cells since the gas volume measurement relies on the expansion measurement of the gas bag. For other cell formats, measurement setups for inline gas detection must be adapted and validated accordingly. For prismatic hardcase and large cylindrical cells, gas flow measurements might be feasible alternatives since these cells are often formed in an open state. Open refers to a configuration in which evolved gases can be released through a hole (e.g., the filling port) in the lid. However, most battery manufacturers have a research lab in addition to a factory, in which pouch cells are frequently built. The reason lies in the simpler manufacturability and greater flexibility of the pouch cell format. Thus, the CEB can most likely be adapted and applied for several manufacturers and laboratories during the early development phase.

A key element within this dissertation was the CEB to optimize the formation protocols since the formation is among the most time-consuming and costly process steps in battery production (WOOD ET AL. 2015b). While aging and EOL tests show a high similarity for different material systems, the formation must be specifically adapted for electrode materials, separators, electrolytes, and cell designs (SCHOMBURG ET AL. 2024). While the functionality of the CEB has been shown for two different material combinations (NMC/graphite and NCA/Si-Gr), the optimization of the formation protocol in P5 has been validated using NMC/graphite cells only. A relatively fast and stable formation of the SEI has been reported for graphite anodes that can be tracked using EIS (SOLCHENBACH ET AL. 2021). For silicon-containing anodes, the SEI formation and gas evolution continue over multiple cycles, making it more challenging to define a termination criterion. However, the CEB allows quantification of the gassing and expansion behavior over a long observation time, and the methodology can be adopted easily. The

transferability of the methodology to silicon-containing LIBs or sodium-ion batteries is thus very promising.

Similarly, all cycle life prediction studies were performed using a NMC/graphite material combination. To ensure transferability, a comprehensive methodology based on the established CRISP-DM approach was developed. Since the data obtained from cell finalization and cycle life testing are similar for different material systems, a simple transferability is expected. However, the features exhibiting the highest correlation will likely vary for other material systems. The transferability is supported by the literature, in which different RUL prediction approaches were also developed for LFP chemistries (SEVERSON ET AL. 2019).

A key challenge for all applications within the ML and DL domain is the number and quality of available data sets (cf. Section 3.3). While the quality in terms of completeness and consistency was provided within all publications, the number of LIBs was limited. This is due to the high costs of battery production at the pilot scale and the limitation in production capability as well as material availability. P3 and P4 were thus limited to a total number of 29 available cells. Hence, overfitting was detected on multiple occasions, which decreased the predictive power of the models. Increasing the number of cells to industrial numbers is believed to significantly improve classification and prediction accuracy. However, since battery manufacturers do not provide data sets publicly, the application in a large-scale production environment is difficult to demonstrate in academia.

Lastly, feature extraction was limited to data sets from cell finalization and testing. This limitation was deliberately chosen since the intention was to provide an easily transferable methodology that does not rely on comprehensive inline measuring equipment. Especially features from electrical data during formation and testing are readily available, as most plants automatically provide the data sets for process control systems or databases. Furthermore, the aim was to assess the cell quality regarding the achievable cycle life rather than the quality of the intermediate products. However, production data from electrode manufacturing and cell assembly might be valuable feature sources to further increase the prediction accuracy. Enabling the integration of comprehensive production data sets within the ML models could also reveal interdependencies within manufacturing that were not within the scope of this dissertation.

5 Summary and Outlook

This chapter presents the conclusion of the dissertation by summarizing the key findings in Section 5.1 and by providing an outlook for future research within the elucidated topics in Section 5.2.

5.1 Summary

LIBs are a cornerstone for modern society and indispensable energy storage devices for consumer products as well as the mobility sector. Especially BEVs rely on high-quality LIBs to compete with conventional combustion vehicles regarding driving range and vehicle costs. Both cell quality and manufacturing costs are greatly influenced by cell finalization due to the time-intensive formation procedure and quality assurance measures. This results from complex electrochemical processes occurring during formation and the difficulty of assessing cell quality in production. To address these issues, novel data-driven approaches were introduced in this dissertation for tailoring formation procedures and enabling early cycle life prediction with the overall goal of accelerating as well as securing process development in cell finalization.

To achieve this goal, multiple studies and analyses were conducted based on the research methodology from BLESSING & CHAKRABARTI (2009). This included a review-based research clarification in Chapter 1 and Chapter 2. After defining the objective and the framework, fundamentals regarding LIBs, as well as ML and AI, were presented. The emphasis was on providing information on the cell-internal processes, such as SEI formation and gas evolution, which occur during the formation of LIBs and restrict the processing speed. Furthermore, fundamentals on battery production and quality assurance measures were provided in Chapter 2. The final ML section aimed to provide the basic concepts, definitions, and methodologies for the later investigations.

The state of the art was subsequently addressed in the comprehensive descriptive study I within Chapter 3, which covered three main topics: formation process, gas evolution detection, and cycle life prediction. In all topics, a need for data-driven product and process analysis was concluded to either improve the process understanding or reduce processing time. A research gap was consequently derived with the overarching aim to expedite and secure process development in cell finalization. To address this aim and close the research gap, four SOs were identified for the dissertation:

- SO1: Development of a comprehensive production concept for tracking the quality-determining product and process parameters

- SO2: Identification of cell-internal processes during formation by operando gassing analysis
- SO3: Advancement of ML approaches to predict the cycle life of a LIB using data from cell finalization
- SO4: Development of a methodology for optimizing and securing formation protocols using operando gassing analysis and cycle life prediction

The SOs were addressed in five publications (P1 – P5) within a comprehensive predictive study in Chapter 4. First, a novel production concept was developed in P1 that included several sensors to improve the product and process understanding during cell finalization. A central target was the identification of non-value-adding processing time and the design of a lean, cell-specific process flow. The production concept also provided the basis for a CPS by linking the sensors to a virtual production system, in which multiple quality parameters can be assessed and evaluated in real time. The gas evolution is an essential parameter to reduce the formation time, as it indicates the SEI formation. To track the gas evolution, a CEB was developed and validated in P2 to detect the gas volume in the pouch bag without interference with the cell setup. The CEB enabled the identification of gas-evolving potential ranges to provide an insight into the cell-internal processes during formation. It was shown that silicon-containing anodes require significantly higher formation times and that pure graphite anodes exhibited gas evolution within the first cycle only.

The consistent tracking of quality parameters during cell finalization established in P1 was the baseline for the ML approach to predict the cycle life of a LIB. A methodology was proposed in P3 to extract features from multiple data sources using a tailored CRISP-DM approach. Furthermore, feature selection and sensitivity studies were performed to confine valuable information sources during production and testing. P4 complemented the methodology by evaluating different modeling approaches based on linear regression and ANNs. The study showed that cycle life prediction using production data is sufficient for detecting defective cells and that quality grades are distinguishable when early cycling data is used. In the final study, P5, the cycle life prediction approach was utilized to advance the formation process efficiently. Two time-reduced formation protocols were derived from the inline gas analysis using the CEB, and multiple quality parameters were tracked during cell finalization. The superior protocol could be identified through feature extraction and subsequent cycle life prediction requiring less than 10 % of the regular testing time, resulting in a minimum formation time of 2.4 h. This highlights the great potential of using data-driven approaches for process development and quality assurance in cell finalization.

Finally, an initial descriptive study II was conducted in Chapter 4 and Chapter 5 that comprised the novel methodology developed in P5 and a critical discussion of the results. The discussion included an evaluation of the novelty of the findings, their contribution to the state of the art, and a critical reflection. It was asserted that the results provide valuable contributions to the research fields, particularly regarding the formation procedure and utilization of ML for cycle life prediction. Tailoring the formation according to the gassing behavior was shown to be a promising approach to reduce processing time while maintaining the overall cell quality.

Furthermore, a pioneering approach was developed to utilize production data from cell finalization to predict the LIB cycle life. Both academic research and industry benefit from the findings, since the approaches are easily applicable, scalable, and material-independent. The unresolved questions identified in the critical discussion offer the opportunity to expand and verify the established knowledge base in subsequent studies.

5.2 Outlook

This dissertation introduced several new approaches regarding the process design and quality assurance in cell finalization. While these approaches have demonstrated significant potentials, additional research can be conducted to further refine the approaches and ensure the transfer into the industry.

Although the concept of operando gassing detection is universal, the CEB was only developed and validated for pouch cells of one specific format. Since multiple manufacturers increasingly use cylindrical cell-type formats, a transfer and adaptation of the measurement principle represents a promising application case. A possibility lies in the meticulous tracking of the gas flow during formation since large cylindrical cells are analogous to prismatic cells formed openly, and the produced gases are continuously extracted from the cell. Installing a precise gas flow sensor in the outlet could enable inline gassing detection and might be integrable in a scaled production line. Furthermore, a calibration measurement was required for the CEB to correlate the displacement of the gas bag to the gas volume, which is challenging if the exact void volumes and cell dimensions are unknown. A finite element method could be a valuable tool to better model the expansion of the gas bag and to account for variations in the cell dimensions. A further opportunity for improvement arises from the semi-automatic production chain at the *iwb*, in which the pouch foil cutting and sealing processes were conducted manually, resulting in varying dimensions of the pouch bag. The reproducibility of the gas detection measurement is expected to improve if fully automated processes are used to cut and seal the pouch foil, offering even more consistent results.

A central limitation of the predictive power of the ML models was the small sample size of approximately 30 cells per configuration. The number of cells should be increased to unveil the full potential of ML or AI. Industrial manufacturers could use several thousand data sets from production since electrical data from formation, aging, or EOL testing is already available from the production equipment. However, initial cycle life testing of a significant number of produced cells to train the models is still required in order to define a baseline quality. An additional challenge for research is that industrial formation or testing data is very difficult to obtain since it contains delicate information about the LIB and is thus commonly disclosed. Hence, academic research on pilot lines is essential to bridge this knowledge gap from laboratory research to the industry. Another possibility for research to improve the database is the utilization of data augmentation techniques. Data augmentation is a ML technique to create additional training data samples using transformation algorithms. Moreover, data from the whole production chain might be used in the future to predict the cell quality and identify product as well as process interdependencies. Nevertheless, this requires a high degree of digitalization during

manufacturing and a continuous tracking of product as well as process parameters using tracking and tracing procedures.

The approach of adapting formation protocols based on the gas evolution showed promising results for NMC/graphite chemistries. An application for other cell chemistries (e.g., for anodes with a high silicon content) is desirable since the formation is typically longer and less understood for Si-Gr blends. Therefore, the operando gas analysis could help to increase the understanding of the cell-internal processes for novel materials by revealing the gas-evolving potential ranges. Further research should also target the non-gaseous SEI formation observed in the EIS measurements at elevated potentials. Conducting the degassing step shortly after the gas evolution termination decreased the formation time drastically, but a potential consolidation of the SEI during subsequent cycling needs to be evaluated. Overall, the formation process remains a challenging, yet rewarding area of focus in battery production. The insights gained from this research provide a solid foundation for future work, which holds the promise of driving significant advancements in both academic and industrial settings.

Bibliography

AIKEN ET AL. 2014
Aiken, C. P.; Xia, J.; Wang, D. Y.; Stevens, D. A.; Trussler, S.; Dahn, J. R.: An Apparatus for the Study of In Situ Gas Evolution in Li-Ion Pouch Cells. Journal of The Electrochemical Society 161 (2014) 10, A1548-A1554, https://doi.org/10.1149/2.0151410jes.

ALSHEIMER ET AL. 2023
Alsheimer, L.; Heidrich, B.; Peschel, C.; Dienwiebel, I.; Winter, M.; Börner, M.: Suppressing gas evolution in Li4Ti5O12-based pouch cells by high temperature formation. Journal of Power Sources 575 (2023), p. 233207, https://doi.org/10.1016/j.jpowsour.2023.233207.

AN ET AL. 2016
An, S. J.; Li, J.; Daniel, C.; Mohanty, D.; Nagpure, S.; Wood, D. L.: The state of understanding of the lithium-ion-battery graphite solid electrolyte interphase (SEI) and its relationship to formation cycling. Carbon 105 (2016), p. 52-76, https://doi.org/10.1016/j.carbon.2016.04.008.

AN ET AL. 2017
An, S. J.; Li, J.; Du, Z.; Daniel, C.; Wood, D. L.: Fast formation cycling for lithium ion batteries. Journal of Power Sources 342 (2017), p. 846-852, https://doi.org/10.1016/j.jpowsour.2017.01.011.

ANDRE ET AL. 2015
Andre, D.; Kim, S.-J.; Lamp, P.; Lux, S. F.; Maglia, F.; Paschos, O.; Stiaszny, B.: Future generations of cathode materials: an automotive industry perspective. Journal of Materials Chemistry A 3 (2015) 13, p. 6709-6732, https://doi.org/10.1039/C5TA00361J.

ANK ET AL. 2023
Ank, M.; Stock, S.; Wassiliadis, N.; Burger, T.; Daub, R.; Lienkamp, M.: Influence analysis of production defects of lithium-ion cells using single-cell and multi-cell characterization. Journal of Energy Storage 62 (2023), p. 106938, https://doi.org/10.1016/j.est.2023.106938.

ANSARI ET AL. 2022
Ansari, S.; Ayob, A.; Hossain Lipu, M. S.; Hussain, A.; Saad, M. H.: Remaining useful life prediction for lithium-ion battery storage system: A comprehensive review of methods, key factors, issues and future outlook. Energy Reports 8 (2022), p. 12153-12185, https://doi.org/10.1016/j.egyr.2022.09.043.

ARORA ET AL. 1999
Arora, P.; Doyle, M.; White, R. E.: Mathematical Modeling of the Lithium Deposition Overcharge Reaction in Lithium‐Ion Batteries Using Carbon‐Based Negative Electrodes. Journal of The Electrochemical Society 146 (1999) 10, p. 3543-3553, https://doi.org/10.1149/1.1392512.

AURBACH ET AL. 1996
Aurbach, D.; Markovsky, B.; Shechter, A.; Ein‐Eli, Y.; Cohen, H.: A Comparative Study of Synthetic Graphite and Li Electrodes in Electrolyte Solutions Based on Ethylene Carbonate‐Dimethyl Carbonate Mixtures. Journal of The Electrochemical Society 143 (1996) 12, p. 3809, https://doi.org/10.1149/1.1837300.

AURBACH ET AL. 2002
Aurbach, D.; Gamolsky, K.; Markovsky, B.; Gofer, Y.; Schmidt, MM Heider, U: On the use of vinylene carbonate (VC) as an additive to electrolyte solutions for Li-ion batteries. Electrochimica Acta 47 (2002) 9, p. 1423-1439, https://doi.org/10.1016/S0013-4686(01)00858-1.

BAR‐TOW ET AL. 1999
Bar‐Tow, D.; Peled, E.; Burstein, L.: A Study of Highly Oriented Pyrolytic Graphite as a Model for the Graphite Anode in Li‐Ion Batteries. Journal of The Electrochemical Society 146 (1999) 3, p. 824, https://doi.org/10.1149/1.1391688.

BERKES ET AL. 2015
Berkes, B. B.; Jozwiuk, A.; Vračar, M.; Sommer, H.; Brezesinski, T.; Janek, J.: Online Continuous Flow Differential Electrochemical Mass Spectrometry with a Realistic Battery Setup for High-Precision, Long-Term Cycling Tests. Analytical chemistry 87 (2015) 12, p. 5878-5883, https://doi.org/10.1021/acs.analchem.5b01237.

BERNHARD ET AL. 2015a
Bernhard, R.; Metzger, M.; Gasteiger, H. A.: Gas Evolution at Graphite Anodes Depending on Electrolyte Water Content and SEI Quality Studied by On-Line Electrochemical Mass Spectrometry. Journal of The Electrochemical Society 162 (2015) 10, A1984-A1989, https://doi.org/10.1149/2.0191510jes.

BERNHARD ET AL. 2015b
Bernhard, R.; Metzger, M.; Gasteiger, H. A.: Gas Evolution at Graphite Anodes Depending on Electrolyte Water Content and SEI Quality Studied by On-Line Electrochemical Mass Spectrometry. Journal of The Electrochemical Society 162 (2015) 10, A1984-A1989, https://doi.org/10.1149/2.0191510jes.

BLESSING & CHAKRABARTI 2009
Blessing, L. T.; Chakrabarti, A.: DRM, a Design Research Methodology. London: Springer London 2009. ISBN: 978-1-84882-586-4.

BLOOM ET AL. 2001
Bloom, I.; Cole, B.; Sohn, J.; Jones, S.; Polzin, E.; Battaglia, V.; Henriksen, G.; Motloch, C.;Richardson, R.; Unkelhaeuser, T.; Ingersoll, D.; Case, H.L: An accelerated calendar and cycle life study of Li-ion cells. Journal of Power Sources 101 (2001) 2, p. 238-247, https://doi.org/10.1016/S0378-7753(01)00783-2.

BRATSCH 1989
Bratsch, S. G.: Standard electrode potentials and temperature coefficients in water at 298.15 K. Journal of Physical and Chemical Reference Data 1 (1989) 18, p. 1-21, https://doi.org/10.1063/1.555839.

BUQA ET AL. 2006
Buqa, H.; Würsig, A.; Vetter, J.; Spahr, M. E.; Krumeich, F.; Novák, P.: SEI film formation on highly crystalline graphitic materials in lithium-ion batteries. Journal of Power Sources 153 (2006) 2, p. 385-390, https://doi.org/10.1016/j.jpowsour.2005.05.036.

BURNS ET AL. 2013
Burns, J. C.; Petibon, R.; Nelson, K. J.; Sinha, N. N.; Kassam, A.; Way, B. M.; Dahn, J. R.: Studies of the Effect of Varying Vinylene Carbonate (VC) Content in Lithium Ion Cells on Cycling Performance and Cell Impedance. Journal of The Electrochemical Society 160 (2013) 10, A1668, https://doi.org/10.1149/2.031310jes.

CHAPMAN ET AL. 2000
Chapman, P.; Clinton, J.; Kerber, R.; Khabaza, T.; Reinartz, T.; Shearer, C.; Wirth, R.: CRISP-DM 1.0: Step-by-step data mining guide. SPSS inc 9 (2000) 13, p. 1-73,

CHENG ET AL. 2015
Cheng, Y.; Lu, C.; Li, T.; Tao, L.: Residual lifetime prediction for lithium-ion battery based on functional principal component analysis and Bayesian approach. Energy 90 (2015), p. 1983-1993, https://doi.org/10.1016/j.energy.2015.07.022.

CHRISTENSEN & NEWMAN 2004
Christensen, J.; Newman, J.: A Mathematical Model for the Lithium-Ion Negative Electrode Solid Electrolyte Interphase. Journal of The Electrochemical Society 151 (2004) 11, A1977, https://doi.org/10.1149/1.1804812.

CORTES & VAPNIK 1995
Cortes, C.; Vapnik, V.: Support-vector networks. Machine learning 20 (1995), p. 273-297,

DIETZ ET AL. 2020
Dietz, T.; Shwom, R. L.; Whitley, C. T.: Climate change and society. Annual Review of Sociology 46 (2020), p. 135-158.

DIN 40729-05
DIN 40729-05: Accumulators; galvanic secondary cells; general terms and definitions. Berlin: Beuth Verlag GmbH 1985.

DIN EN ISO 16773-1
DIN EN ISO 16773-1: Electrochemical impedance spectroscopy (EIS) on coated and uncoated metallic specimens. Berlin: Beuth Verlag GmbH 2019.

DIN EN IEC 62660-1
DIN EN IEC 62660-1: Secondary lithium-ion cells for the propulsion of electric road vehicles. Berlin: Beuth Verlag GmbH 2019.

DREES ET AL. 2021
Drees, R.; Lienesch, F.; Kurrat, M.: Fast charging lithium-ion battery formation based on simulations with an electrode equivalent circuit model. Journal of Energy Storage 36 (2021) 102345. https://doi.org/10.1016/j.est.2021.102345.

DREES ET AL. 2023
Drees, R.; Lienesch, F.; Kurrat, M.: Fast Charging Formation of Lithium‐Ion Batteries Based on Real‐Time Negative Electrode Voltage Control. Energy Technology 11 (2023) 5, p. 2200868, https://doi.org/10.1002/ente.202200868.

DUBARRY ET AL. 2010
Dubarry, M.; Vuillaume, N.; Liaw, B. Y.: Origins and accommodation of cell variations in Li-ion battery pack modeling. International Journal of Energy Research 34 (2010) 2, p. 216-231, https://doi.org/10.1002/er.1668.

ELDESOKY ET AL. 2021
Eldesoky, A.; Bauer, M.; Azam, S.; Zsoldos, E.; Song, W.; Weber, R.; Hy, S.; Johnson, M. B.;Metzger, Michael; Dahn, J. R.: Impact of Graphite Materials on the Lifetime of NMC811/Graphite Pouch Cells: Part I. Material Properties, ARC Safety Tests, Gas Generation, and Room Temperature Cycling. Journal of The Electrochemical Society 168 (2021) 11, p. 110543, https://doi.org/10.1149/1945-7111/ac39fc.

ELDESOKY ET AL. 2022
Eldesoky, A.; Logan, E. R.; Louli, A. J.; Song, W.; Weber, R.; Hy, S.; Petibon, R.; Harlow, J. E.;Azam, S.; Zsoldos, E.; Dahn, J. R.: Impact of Graphite Materials on the Lifetime of NMC811/Graphite Pouch Cells: Part II. Long-Term Cycling, Stack Pressure Growth, Isothermal Microcalorimetry, and Lifetime Projection. Journal of The Electrochemical Society 169 (2022) 1, p. 10501, https://doi.org/10.1149/1945-7111/ac42f1.

ELMAHALLAWY ET AL. 2022
Elmahallawy, M.; Elfouly, T.; Alouani, A.; Massoud, A. M.: A Comprehensive Review of Lithium-Ion Batteries Modeling, and State of Health and Remaining Useful Lifetime Prediction. IEEE Access 10 (2022), p. 119040-119070, https://doi.org/10.1109/ACCESS.2022.3221137.

FENG ET AL. 2018
Feng, K.; Li, M.; Liu, W.; Kashkooli, A. G.; Xiao, X.; Cai, M.; Chen, Z.: Silicon-Based Anodes for Lithium-Ion Batteries: From Fundamentals to Practical Applications. Small (Weinheim an der Bergstrasse, Germany) 14 (2018) 8. https://doi.org/10.1002/smll.201702737.

FLEISCHMANN ET AL. 2023
Fleischmann, J.; Hanicke, M.; Horetsky, E.; Ibrahim, D.; Jautelat, S.; Linder, M.; Schaufuss, P.; Torscht, L.; van de Rijt, Alexandre: Battery 2030: Resilient, sustainable, and circular. McKinsey & Company (2023), p. 2-18,

FROCHTE 2019
Frochte, J.: Maschinelles Lernen. Grundlagen und Algorithmen in Python. 2., aktualisierte Auflage. München: Hanser 2019. ISBN: 978-3-446-45996-0.

GENG ET AL. 2020
Geng, L.; Wood, D. L.; Lewis, S. A.; Connatser, R. M.; Li, M.; Jafta, C. J.; Belharouak, I.: High accuracy in-situ direct gas analysis of Li-ion batteries. Journal of Power Sources 466 (2020), p. 228211, https://doi.org/10.1016/j.jpowsour.2020.228211.

GÉRON 2019
Géron, A.: Hands-on machine learning with Scikit-Learn, Keras, and TensorFlow. Concepts, tools, and techniques to build intelligent systems. Second edition. Beijing China, Sebastopol CA: O'Reilly Media Inc 2019. ISBN: 9781492032649.

GRAF 2018
Graf, C.: Cathode materials for lithium-ion batteries. In: Korthauer, R. (Hrsg.): Lithium-Ion Batteries: Basics and Applications. Berlin, Heidelberg: Springer Berlin Heidelberg 2018, p. 29-42. ISBN: 978-3-662-53069-6.

GÜNTER ET AL. 2019
Günter, F. J.; Burgstaller, C.; Konwitschny, F.; Reinhart, G.: Influence of the Electrolyte Quantity on Lithium-Ion Cells. Journal of The Electrochemical Society 166 (2019) 10, A1709-A1714, https://doi.org/10.1149/2.0121910jes.

HARRIS ET AL. 2020
Harris, O. C.; Lee, S. E.; Lees, C.; Tang, M.: Review: mechanisms and consequences of chemical cross-talk in advanced Li-ion batteries. Journal of Physics: Energy 2 (2020) 3, p. 32002, https://doi.org/10.1088/2515-7655/ab8b68.

HARTNIG & SCHMIDT 2018
Hartnig, C.; Schmidt, M.: Electrolytes and conducting salts. In: Korthauer, R. (Hrsg.): Lithium-Ion Batteries: Basics and Applications. Berlin, Heidelberg: Springer Berlin Heidelberg 2018, p. 59-74. ISBN: 978-3-662-53069-6.

HAWLEY & LI 2019
Hawley, W. B.; Li, J.: Electrode manufacturing for lithium-ion batteries—Analysis of current and next generation processing. Journal of Energy Storage 25 (2019), p. 100862, https://doi.org/10.1016/j.est.2019.100862.

HEIMES ET AL. 2020
Heimes, H. H.; Offermanns, C.; Mohsseni, A.; Laufen, H.; Westerhoff, U.; Hoffmann, L.; Niehoff, P.; Kurrat, M.;Winter, Martin; Kampker, Achim: The Effects of Mechanical and Thermal Loads during Lithium‐Ion Pouch Cell Formation and Their Impacts on Process Time. Energy Technology 8 (2020) 2, p. 1900118, https://doi.org/10.1002/ente.201900118.

HEISKANEN ET AL. 2019
Heiskanen, S. K.; Kim, J.; Lucht, B. L.: Generation and Evolution of the Solid Electrolyte Interphase of Lithium-Ion Batteries. Joule 3 (2019) 10, p. 2322-2333, https://doi.org/10.1016/j.joule.2019.08.018.

HU ET AL. 2014
Hu, C.; Jain, G.; Tamirisa, P.; Gorka, T.: Method for estimating capacity and predicting remaining useful life of lithium-ion battery. Applied Energy 126 (2014), p. 182-189, https://doi.org/10.1016/j.apenergy.2014.03.086.

IMHOF & NOVÁK 1998
Imhof, R.; Novák, P.: In Situ Investigation of the Electrochemical Reduction of Carbonate Electrolyte Solutions at Graphite Electrodes. Journal of The Electrochemical Society 145 (1998), p. 1081-1087,

JEONG ET AL. 2001
Jeong, S.-K.; Inaba, M.; Abe, T.; Ogumi, Z.: Surface Film Formation on Graphite Negative Electrode in Lithium-Ion Batteries. Journal of The Electrochemical Society 148 (2001) 9, p. 989-993, https://doi.org/10.1149/1.1387981.

JIANG ET AL. 2021
Jiang, B.; Gent, W. E.; Mohr, F.; Das, S.; Berliner, M. D.; Forsuelo, M.; Zhao, H.; Attia, P. M.;Grover, Aditya; Herring, Patrick K.; Bazant, Martin Z.; Harris, Stephen J.; Ermon, Stefano; Chueh, William C.; Braatz, Richard D.: Bayesian learning for rapid prediction of lithium-ion battery-cycling protocols. Joule 5 (2021) 12, p. 3187-3203, https://doi.org/10.1016/j.joule.2021.10.010.

JOSHI 2020
Joshi, A. V.: Machine Learning and Artificial Intelligence. Cham: Springer International Publishing 2020. ISBN: 978-3-030-26621-9.

KIM ET AL. 2011
Kim, S.-P.; van Duin, A. C.; Shenoy, V. B.: Effect of electrolytes on the structure and evolution of the solid electrolyte interphase (SEI) in Li-ion batteries: A molecular dynamics study. Journal of Power Sources 196 (2011) 20, p. 8590-8597, https://doi.org/10.1016/j.jpowsour.2011.05.061.

KIM ET AL. 2023
Kim, S.; Kim, H.-S.; Kim, B.; Kim, Y.-J.; Jung, J.-W.; Ryu, W.-H.: In Situ Gas Analysis by Differential Electrochemical Mass Spectrometry for Advanced Rechargeable Batteries: A Review. Advanced Energy Materials 13 (2023) 39. https://doi.org/10.1002/aenm.202301983.

KIM & LEE 2020
Kim, H.-K.; Lee, K.-J.: Scale-Up of Physics-Based Models for Predicting Degradation of Large Lithium Ion Batteries. Sustainability 12 (2020) 20, p. 8544, https://doi.org/10.3390/su12208544.

KOLETI ET AL. 2021
Koleti, U. R.; Bui, T. N.; Dinh, T. Q.; Marco, J.: The Development of Optimal Charging Protocols for Lithium-Ion Batteries to Reduce Lithium Plating. Journal of Energy Storage 39 (2021), p. 102573, https://doi.org/10.1016/j.est.2021.102573.

KURFER ET AL. 2012
Kurfer, J.; Westermeier, M.; Tammer, C.; Reinhart, G.: Production of large-area lithium-ion cells – Preconditioning, cell stacking and quality assurance. CIRP Annals 61 (2012) 1, p. 1-4, https://doi.org/10.1016/j.cirp.2012.03.101.

KURZWEIL & DIETLMEIER 2018
Kurzweil, P.; Dietlmeier, O. K.: Elektrochemische Speicher. Wiesbaden: Springer Fachmedien Wiesbaden 2018. ISBN: 978-3-658-21828-7.

KWADE ET AL. 2018
Kwade, A.; Haselrieder, W.; Leithoff, R.; Modlinger, A.; Dietrich, F.; Droeder, K.: Current status and challenges for automotive battery production technologies. Nature Energy 3 (2018) 4, p. 290-300, https://doi.org/10.1038/s41560-018-0130-3.

LAMB ET AL. 2021
Lamb, W. F.; Wiedmann, T.; Pongratz, J.; Andrew, R.; Crippa, M.; Olivier, J. G.; Wiedenhofer, D.; Mattioli, G.;Khourdajie, Alaa Al; House, Jo; Pachauri, Shonali; Figueroa, Maria; Saheb, Yamina; Slade, Raphael; Hubacek, Klaus; Sun, Laixiang; Ribeiro, Suzana Kahn; Khennas, Smail; La Rue Can, Stephane de; Chapungu, Lazarus; Davis, Steven J.; Bashmakov, Igor; Dai, Hancheng; Dhakal, Shobhakar; Tan, Xianchun; Geng, Yong; Gu, Baihe; Minx, Jan: A review of trends and drivers of greenhouse gas emissions by sector from 1990 to 2018. Environmental Research Letters 16 (2021) 7, p. 73005, https://doi.org/10.1088/1748-9326/abee4e.

LAMBERT ET AL. 2017
Lambert, S. M.; Armstrong, M.; Attidekou, P. S.; Christensen, P. A.; Widmer, J. D.; Wang, C.; Scott, K.: Rapid Nondestructive-Testing Technique for In-Line Quality Control of Li-Ion Batteries. IEEE Transactions on Industrial Electronics 64 (2017) 5, p. 4017-4026, https://doi.org/10.1109/TIE.2016.2643601.

LANDESFEIND ET AL. 2017
Landesfeind, J.; Pritzl, D.; Gasteiger, H. A.: An Analysis Protocol for Three-Electrode Li-Ion Battery Impedance Spectra: Part I. Analysis of a High-Voltage Positive Electrode. Journal of The Electrochemical Society 164 (2017) 7, A1773-A1783, https://doi.org/10.1149/2.0131709jes.

LEE ET AL. 2004
Lee, H.-H.; Wang, Y.-Y.; Wan, C.-C.; Yang, M.-H.; Wu, H.-C.; Shieh, D.-T.: A fast formation process for lithium batteries. Journal of Power Sources 134 (2004) 1, p. 118-123, https://doi.org/10.1016/j.jpowsour.2004.03.020.

LEE ET AL. 2022
Lee, D.; Kim, B.; Shin, C. B.: Modeling Fast Charge Protocols to Prevent Lithium Plating in a Lithium-Ion Battery. Journal of The Electrochemical Society 169 (2022) 9, p. 90502, https://doi.org/10.1149/1945-7111/ac89b6.

LEIßING ET AL. 2020
Leißing, M.; Winter, M.; Wiemers-Meyer, S.; Nowak, S.: A method for quantitative analysis of gases evolving during formation applied on LiNi0.6Mn0.2Co0.2O2 || natural graphite lithium ion battery cells using gas chromatography - barrier discharge ionization detector. Journal of chromatography. A 1622 (2020), p. 461122, https://doi.org/10.1016/j.chroma.2020.461122.

LEUTHNER 2018
Leuthner, S.: Lithium-ion battery overview. In: Korthauer, R. (Hrsg.): Lithium-Ion Batteries: Basics and Applications. Berlin, Heidelberg: Springer Berlin Heidelberg 2018, p. 13-20. ISBN: 978-3-662-53069-6.

LIU ET AL. 2021
Liu, Y.; Zhang, R.; Wang, J.; Wang, Y.: Current and future lithium-ion battery manufacturing. iScience 24 (2021) 4, p. 102332, https://doi.org/10.1016/j.isci.2021.102332.

LU ET AL. 2014
Lu, P.; Li, C.; Schneider, E. W.; Harris, S. J.: Chemistry, Impedance, and Morphology Evolution in Solid Electrolyte Interphase Films during Formation in Lithium Ion Batteries. The Journal of Physical Chemistry C 118 (2014) 2, p. 896-903, https://doi.org/10.1021/jp4111019.

MAO ET AL. 2018
Mao, C.; An, S. J.; Meyer, H. M.; Li, J.; Wood, M.; Ruther, R. E.; Wood, D. L.: Balancing formation time and electrochemical performance of high energy lithium-ion batteries. Journal of Power Sources 402 (2018), p. 107-115, https://doi.org/10.1016/j.jpowsour.2018.09.019.

MAO ET AL. 2019
Mao, C.; Ruther, R. E.; Geng, L.; Li, Z.; Leonard, D. N.; Meyer, H. M.; Sacci, R. L.; Wood, D. L.: Evaluation of Gas Formation and Consumption Driven by Crossover Effect in High-Voltage Lithium-Ion Batteries with Ni-Rich NMC Cathodes. ACS applied materials & interfaces 11 (2019) 46, p. 43235-43243, https://doi.org/10.1021/acsami.9b15916.

MÄRKLE ET AL. 2011
Märkle, W.; Lu, C.-Y.; Novák, P.: Morphology of the Solid Electrolyte Interphase on Graphite in Dependency on the Formation Current. Journal of The Electrochemical Society 158 (2011) 12, A1478, https://doi.org/10.1149/2.077112jes.

MATTINEN ET AL. 2020
Mattinen, U.; Klett, M.; Lindbergh, G.; Wreland Lindström, R.: Gas evolution in commercial Li-ion battery cells measured by on-line mass spectrometry – Effects of C-rate and cell voltage. Journal of Power Sources 477 (2020), p. 228968, https://doi.org/10.1016/j.jpowsour.2020.228968.

METZGER ET AL. 2016
Metzger, M.; Strehle, B.; Solchenbach, S.; Gasteiger, H. A.: Hydrolysis of Ethylene Carbonate with Water and Hydroxide under Battery Operating Conditions. Journal of The Electrochemical Society 163 (2016) 7, A1219-A1225, https://doi.org/10.1149/2.0411607jes.

MIAO ET AL. 2013
Miao, Q.; Xie, L.; Cui, H.; Liang, W.; Pecht, M.: Remaining useful life prediction of lithium-ion battery with unscented particle filter technique. Microelectronics Reliability 53 (2013) 6, p. 805-810, https://doi.org/10.1016/j.microrel.2012.12.004.

MICHALAK ET AL. 2015
Michalak, B.; Sommer, H.; Mannes, D.; Kaestner, A.; Brezesinski, T.; Janek, J.: Gas Evolution in Operating Lithium-Ion Batteries Studied In Situ by Neutron Imaging. Scientific reports 5 (2015), p. 15627, https://doi.org/10.1038/srep15627.

MISIEWICZ ET AL. 2023
Misiewicz, C.; Lundström, R.; Ahmed, I.; Lacey, M. J.; Brant, W. R.; Berg, E. J.: Online electrochemical mass spectrometry on large-format Li-ion cells. Journal of Power Sources 554 (2023), p. 232318, https://doi.org/10.1016/j.jpowsour.2022.232318.

MÜLLER ET AL. 2018
Müller, V.; Kaiser, R.; Poller, S.; Sauerteig, D.: Importance of the constant voltage charging step during lithium-ion cell formation. Journal of Energy Storage 15 (2018), p. 256-265, https://doi.org/10.1016/j.est.2017.11.020.

NUHIC ET AL. 2013
Nuhic, A.; Terzimehic, T.; Soczka-Guth, T.; Buchholz, M.; Dietmayer, K.: Health diagnosis and remaining useful life prognostics of lithium-ion batteries using data-driven methods. Journal of Power Sources 239 (2013), p. 680-688, https://doi.org/10.1016/j.jpowsour.2012.11.146.

ONUKI ET AL. 2008
Onuki, M.; Kinoshita, S.; Sakata, Y.; Yanagidate, M.; Otake, Y.; Ue, M.; Deguchi, M.: Identification of the Source of Evolved Gas in Li-Ion Batteries Using #2#1 -labeled Solvents. Journal of The Electrochemical Society 155 (2008) 11, A794, https://doi.org/10.1149/1.2969947.

PELED ET AL. 1998
Peled, E.; Golodnitsky, D.; Menachem, C.; Bar‐Tow, D.: An Advanced Tool for the Selection of Electrolyte Components for Rechargeable Lithium Batteries. Journal of The Electrochemical Society 145 (1998) 10, p. 3482, https://doi.org/10.1149/1.1838831.

PETTINGER ET AL. 2018
Pettinger, K.-H.; Kampker, A.; Hohenthanner, C.-R.; Deutskens, C.; Heimes, H.; vom Hemdt, A.: Lithium-ion cell and battery production processes. In: Korthauer, R. (Hrsg.): Lithium-Ion Batteries: Basics and Applications. Berlin, Heidelberg: Springer Berlin Heidelberg 2018, p. 211-226. ISBN: 978-3-662-53069-6.

PINSON & BAZANT 2013
Pinson, M. B.; Bazant, M. Z.: Theory of SEI Formation in Rechargeable Batteries: Capacity Fade, Accelerated Aging and Lifetime Prediction. Journal of The Electrochemical Society 160 (2013) 2, A243-A250, https://doi.org/10.1149/2.044302jes.

PRITZL ET AL. 2018
Pritzl, D.; Landesfeind, J.; Solchenbach, S.; Gasteiger, H. A.: An Analysis Protocol for Three-Electrode Li-Ion Battery Impedance Spectra: Part II. Analysis of a Graphite Anode Cycled vs. LNMO. Journal of The Electrochemical Society 165 (2018) 10, A2145-A2153, https://doi.org/10.1149/2.0461810jes.

RAGO ET AL. 2019
Rago, N. D.; Basco, J. K.; Vu, A.; Li, J.; Hays, K.; Sheng, Y.; Wood, D. L.; Bloom, I.: Effect of formation protocol: Cells containing Si-Graphite composite electrodes. Journal of Power Sources 435 (2019), p. 126548, https://doi.org/10.1016/j.jpowsour.2019.04.076.

REBALA ET AL. 2019
Rebala, G.; Ravi, A.; Churiwala, S.: An Introduction to Machine Learning. Cham: Springer International Publishing 2019. ISBN: 978-3-030-15728-9.

REINHART ET AL. 2013
Reinhart, G.; Zeilinger, T.; Kurfer, J.; Westermeier, M.; Thiemann, C.; Glonegger, M.; Wunderer, M.; Tammer, C.;Schweier, M.; Heinz, M.: Research and Demonstration Center for the Production of Large-Area Lithium-Ion Cells. In: Schuh, G. et al. (Hrsg.): Future Trends in Production Engineering. Berlin, Heidelberg: Springer Berlin Heidelberg 2013, p. 3-12. ISBN: 978-3-642-24490-2.

REN ET AL. 2018
Ren, L.; Zhao, L.; Hong, S.; Zhao, S.; Wang, H.; Zhang, L.: Remaining Useful Life Prediction for Lithium-Ion Battery: A Deep Learning Approach. IEEE Access 6 (2018), p. 50587-50598, https://doi.org/10.1109/ACCESS.2018.2858856.

RENIERS ET AL. 2019
Reniers, J. M.; Mulder, G.; Howey, D. A.: Review and Performance Comparison of Mechanical-Chemical Degradation Models for Lithium-Ion Batteries. Journal of The Electrochemical Society 166 (2019) 14, A3189-A3200, https://doi.org/10.1149/2.0281914jes.

ROWDEN & GARCIA-ARAEZ 2020
Rowden, B.; Garcia-Araez, N.: A review of gas evolution in lithium ion batteries. Energy Reports 6 (2020), p. 10-18, https://doi.org/10.1016/j.egyr.2020.02.022.

ROYAL SWEDISH ACADEMY OF SCIENCES 2019
Royal Swedish Academy of Sciences: The Nobel Prize in Chemistry 2019. https://www.nobelprize.org/prizes/chemistry/2019/popular-information/ (Accessed: 22.02.2024).

RUSSELL ET AL. 2010
Russell, S. J.; Norvig, P.; Davis, E.: Artificial intelligence. A modern approach. 3rd ed. Upper Saddle River: Prentice Hall 2010. ISBN: 9780136042594.

SAHA ET AL. 2009
Saha, B.; Goebel, K.; Christophersen, J.: Comparison of prognostic algorithms for estimating remaining useful life of batteries. Transactions of the Institute of Measurement and Control 31 (2009) 3-4, p. 293-308, https://doi.org/10.1177/0142331208092030.

SALOMEZ ET AL. 2023
Salomez, B.; Grugeon, S.; Armand, M.; Tran-Van, P.; Laruelle, S.: Review—Gassing Mechanisms in Lithium-ion Battery. Journal of The Electrochemical Society 170 (2023) 5, p. 50537, https://doi.org/10.1149/1945-7111/acd2fd.

SCHMIEGEL ET AL. 2020
Schmiegel, J.-P.; Leißing, M.; Weddeling, F.; Horsthemke, F.; Reiter, J.; Fan, Q.; Nowak, S.; Winter, M.; Placke, Tobias: Novel In Situ Gas Formation Analysis Technique Using a Multilayer Pouch Bag Lithium Ion Cell Equipped with Gas Sampling Port. Journal of The Electrochemical Society 167 (2020) 6, p. 60516, https://doi.org/10.1149/1945-7111/ab8409.

SCHNELL & REINHART 2016
Schnell, J.; Reinhart, G.: Quality Management for Battery Production: A Quality Gate Concept. Procedia CIRP 57 (2016), p. 568-573, https://doi.org/10.1016/j.procir.2016.11.098.

SCHOMBURG ET AL. 2024
Schomburg, F.; Heidrich, B.; Wennemar, S.; Drees, R.; Roth, T.; Kurrat, M.; Heimes, H.; Jossen, A.;Winter, Martin; Cheong, Jun Young; Röder, Fridolin: Lithium-ion battery cell formation: status and future directions towards a knowledge-based process design. Energy & Environmental Science (2024)https://doi.org/10.1039/D3EE03559J.

SCHUSTER ET AL. 2015a
Schuster, S. F.; Brand, M. J.; Berg, P.; Gleissenberger, M.; Jossen, A.: Lithium-ion cell-to-cell variation during battery electric vehicle operation. Journal of Power Sources 297 (2015), p. 242-251, https://doi.org/10.1016/j.jpowsour.2015.08.001.

SCHUSTER ET AL. 2015b
Schuster, S. F.; Bach, T.; Fleder, E.; Müller, J.; Brand, M.; Sextl, G.; Jossen, A.: Nonlinear aging characteristics of lithium-ion cells under different operational conditions. Journal of Energy Storage 1 (2015), p. 44-53, https://doi.org/10.1016/j.est.2015.05.003.

SCHWENKE ET AL. 2019
Schwenke, K. U.; Solchenbach, S.; Demeaux, J.; Lucht, B. L.; Gasteiger, H. A.: The Impact of CO 2 Evolved from VC and FEC during Formation of Graphite Anodes in Lithium-Ion Batteries. Journal of The Electrochemical Society 166 (2019) 10, A2035-A2047, https://doi.org/10.1149/2.0821910jes.

SELF ET AL. 2015
Self, J.; Aiken, C. P.; Petibon, R.; Dahn, J. R.: Survey of Gas Expansion in Li-Ion NMC Pouch Cells. Journal of The Electrochemical Society 162 (2015) 6, A796-A802, https://doi.org/10.1149/2.0081506jes.

SEVERSON ET AL. 2019
Severson, K. A.; Attia, P. M.; Jin, N.; Perkins, N.; Jiang, B.; Yang, Z.; Chen, M. H.; Aykol, M.;Herring, Patrick K.; Fraggedakis, Dimitrios; Bazant, Martin Z.; Harris, Stephen J.; Chueh, William C.; Braatz, Richard D.: Data-driven prediction of battery cycle life before capacity degradation. Nature Energy 4 (2019) 5, p. 383-391, https://doi.org/10.1038/s41560-019-0356-8.

SMOLA & SCHÖLKOPF 2004
Smola, A. J.; Schölkopf, B.: A tutorial on support vector regression. Statistics and Computing 14 (2004) 3, p. 199-222, https://doi.org/10.1023/B:STCO.0000035301.49549.88.

SOLCHENBACH ET AL. 2021
Solchenbach, S.; Huang, X.; Pritzl, D.; Landesfeind, J.; Gasteiger, H. A.: Monitoring SEI Formation on Graphite Electrodes in Lithium-Ion Cells by Impedance Spectroscopy. Journal of The Electrochemical Society 168 (2021) 11, p. 110503, https://doi.org/10.1149/1945-7111/ac3158.

STREICH ET AL. 2017
Streich, D.; Erk, C.; Guéguen, A.; Müller, P.; Chesneau, F.-F.; Berg, E. J.: Operando Monitoring of Early Ni-mediated Surface Reconstruction in Layered Lithiated Ni–Co–Mn Oxides. The Journal of Physical Chemistry C 121 (2017) 25, p. 13481-13486, https://doi.org/10.1021/acs.jpcc.7b02303.

TSIOUVARAS ET AL. 2013
Tsiouvaras, N.; Meini, S.; Buchberger, I.; Gasteiger, H. A.: A Novel On-Line Mass Spectrometer Design for the Study of Multiple Charging Cycles of a Li-O 2 Battery. Journal of The Electrochemical Society 160 (2013) 3, A471-A477, https://doi.org/10.1149/2.042303jes.

TURING 1950
Turing, A. M.: Computing Machinery and Intelligence. Mind 59 (1950) 236, p. 433-460,

VUORILEHTO 2018
Vuorilehto, K.: Materials and function. In: Korthauer, R. (Hrsg.): Lithium-Ion Batteries: Basics and Applications. Berlin, Heidelberg: Springer Berlin Heidelberg 2018, p. 21-28. ISBN: 978-3-662-53069-6.

WALDMANN ET AL. 2018
Waldmann, T.; Hogg, B.-I.; Wohlfahrt-Mehrens, M.: Li plating as unwanted side reaction in commercial Li-ion cells – A review. Journal of Power Sources 384 (2018), p. 107-124, https://doi.org/10.1016/j.jpowsour.2018.02.063.

WANG ET AL. 2018
Wang, A.; Kadam, S.; Li, H.; Shi, S.; Qi, Y.: Review on modeling of the anode solid electrolyte interphase (SEI) for lithium-ion batteries. npj Computational Materials 4 (2018) 1, p. 359, https://doi.org/10.1038/s41524-018-0064-0.

WEBER & ROTH 2018
Weber, C. J.; Roth, M.: Separators. In: Korthauer, R. (Hrsg.): Lithium-Ion Batteries: Basics and Applications. Berlin, Heidelberg: Springer Berlin Heidelberg 2018, p. 75-88. ISBN: 978-3-662-53069-6.

WOOD ET AL. 2015a
Wood, D. L.; Li, J.; Daniel, C.: Prospects for reducing the processing cost of lithium ion batteries. Journal of Power Sources 275 (2015), p. 234-242, https://doi.org/10.1016/j.jpowsour.2014.11.019.

WOOD ET AL. 2015b
Wood, D. L.; Li, J.; Daniel, C.: Prospects for reducing the processing cost of lithium ion batteries. Journal of Power Sources 275 (2015), p. 234-242, https://doi.org/10.1016/j.jpowsour.2014.11.019.

WOOD ET AL. 2019
Wood, D. L.; Li, J.; An, S. J.: Formation Challenges of Lithium-Ion Battery Manufacturing. Joule 3 (2019) 12, p. 2884-2888, https://doi.org/10.1016/j.joule.2019.11.002.

WU ET AL. 2019
Wu, Y.; Li, W.; Wang, Y.; Zhang, K.: Remaining Useful Life Prediction of Lithium-Ion Batteries Using Neural Network and Bat-Based Particle Filter. IEEE Access 7 (2019), p. 54843-54854, https://doi.org/10.1109/ACCESS.2019.2913163.

WURM ET AL. 2018
Wurm, C.; Oettinger, O.; Wittkaemper, S.; Zauter, R.; Vuorilehto, K.: Anode materials for lithium-ion batteries. In: Korthauer, R. (Hrsg.): Lithium-Ion Batteries: Basics and Applications. Berlin, Heidelberg: Springer Berlin Heidelberg 2018, p. 43-58. ISBN: 978-3-662-53069-6.

XIAOYU LI ET AL. 2014
Xiaoyu Li; Tiansi Wang; Lei Pei; Chunbo Zhu; Bingliang Xu: A comparative study of sorting methods for Lithium-ion batteries. (Hrsg.): 2014 IEEE Conference and Expo Transportation Electrification Asia-Pacific (ITEC Asia-Pacific), 2014 IEEE Conference and Expo Transportation Electrification Asia-Pacific (ITEC Asia-Pacific) 2014, p. 1-6,

XIE ET AL. 2020
Xie, L.; Ren, D.; Wang, L.; Chen, Z.; Tian, G.; Amine, K.; He, X.: A Facile Approach to High Precision Detection of Cell-to-Cell Variation for Li-ion Batteries. Scientific reports 10 (2020) 1, p. 7182, https://doi.org/10.1038/s41598-020-64174-2.

XIE & LU 2020
Xie, J.; Lu, Y.-C.: A retrospective on lithium-ion batteries. Nature communications 11 (2020) 1, p. 2499, https://doi.org/10.1038/s41467-020-16259-9.

XU 2004
Xu, K.: Nonaqueous Liquid Electrolytes for Lithium-Based Rechargeable Batteries // Nonaqueous liquid electrolytes for lithium-based rechargeable batteries. Chemical Reviews 104 (2004) 10, p. 4303-4418, https://doi.org/10.1021/cr030203g.

YAN ET AL. 2020
Yan, C.; Yao, Y.-X.; Cai, W.-L.; Xu, L.; Kaskel, S.; Park, H. S.; Huang, J.-Q.: The influence of formation temperature on the solid electrolyte interphase of graphite in lithium ion batteries. Journal of Energy Chemistry 49 (2020), p. 335-338, https://doi.org/10.1016/j.jechem.2020.02.052.

YANG ET AL. 2017
Yang, X.-G.; Leng, Y.; Zhang, G.; Ge, S.; Wang, C.-Y.: Modeling of lithium plating induced aging of lithium-ion batteries: Transition from linear to nonlinear aging. Journal of Power Sources 360 (2017), p. 28-40, https://doi.org/10.1016/j.jpowsour.2017.05.110.

YUE ET AL. 2017a
Yue, X.; Kiely, J.; Ghauri, S.; Kauer, M.; Bellanger, M.; Gibson, D.: A successive approximation method to precisely measure leakage current of the rechargeable Lithium coin battery. Journal of Energy Storage 13 (2017), p. 442-446, https://doi.org/10.1016/j.est.2017.08.006.

YUE ET AL. 2017b
Yue, X.; Kiely, J.; Ghauri, S.; Kauer, M.; Bellanger, M.; Gibson, D.: A successive approximation method to precisely measure leakage current of the rechargeable Lithium coin battery. Journal of Energy Storage 13 (2017), p. 442-446, https://doi.org/10.1016/j.est.2017.08.006.

ZHANG 2006
Zhang, S. S.: A review on electrolyte additives for lithium-ion batteries. Journal of Power Sources 162 (2006) 2, p. 1379-1394, https://doi.org/10.1016/j.jpowsour.2006.07.074.

ZHOU ET AL. 2016
Zhou, Y.; Huang, M.; Chen, Y.; Tao, Y.: A novel health indicator for on-line lithium-ion batteries remaining useful life prediction. Journal of Power Sources 321 (2016), p. 1-10, https://doi.org/10.1016/j.jpowsour.2016.04.119.

ZHU ET AL. 2019
Zhu, S.; Zhao, N.; Sha, J.: Predicting battery life with early cyclic data by machine learning. Energy Storage 1 (2019) 6. https://doi.org/10.1002/est2.98.

Appendix

A List of supervised student research projects

Throughout the course of this dissertation, the author supervised numerous student theses and research projects that were conducted at the *iwb* of the TUM. The collaborative efforts with the students yielded valuable insights, some of which have been integrated into this document as well as the publications. The author sincerely acknowledges the students for their invaluable discussions and the development of ideas during the collaborative process. The supervised theses are listed in chronological order.

CLAUDIA STADLER
Identification of the production environment for the process-specific introduction of additives in the lithium-ion battery production. Bachelor thesis, 2020.

SEBASTIAN POHLMANN
Development of a predictive model for the lifetime estimation of large-size lithium-ion batteries using machine learning. Master thesis, 2020.

MARIA VOß
Development of a cell bracket with pressure sensors for the optimization of the formation process. Semester thesis, 2020.

EDWIN LEE
Development of a lifetime classification model during the formation of lithium-ion batteries using artificial intelligence. Master thesis, 2021.

FELIX DILLER
Implementation of In-Situ-Measurements in the Formation Process of the Lithium-Ion Battery Production. Master thesis, 2021.

MAHMOUD AHMED
Investigation of Machine Learning Techniques for Cycle Life Prediction of Lithium-Ion Batteries. Master thesis, 2021.

TALHA WADOOD
Lifetime Prediction and Classification of Lithium-ion Batteries using Deep Neural Networks. Master thesis, 2022.

BENEDIKT ZELS
Development of a Data Augmentation Model for Cycle Life Prediction of Lithium-ion Batteries. Semester thesis, 2022.

SIMON KAPFER
Enabling the inline measurement of the wetting degree during the filling of lithium-ion batteries. Bachelor thesis, 2022.

AHMED MADY
Data-driven analysis of lithium-ion battery quality in production. Master thesis, 2022.

JONAS BÖHM
Analysis of gas evolution and impedance change during the formation of lithium-ion cells. Bachelor thesis, 2022.

SEBASTIAN ROBEIS
Gassing optimized formation of lithium-ion cells. Bachelor thesis, 2023.

PHILIPP RATH
Investigation of gas generation during formation of lithium-ion batteries for the efficient process design. Master thesis, 2023.

KILIAN SCHEER
Influence of Conductive Salts on Aluminum Current Collector Corrosion and Lifetime of Lithium-Ion Cells. Master thesis, 2024.

JOHANN MEFFERT
Development of a method for the efficient procurement and commissioning of new plant equipment for pilot lines in lithium-ion battery production. Master thesis, 2024.

LHOUSSAINE BOUWADOU
Development of machine learning methods for lithium-ion battery quality prediction and process optimization in cell finalization. Master thesis, 2024.

B Publications of the author

The publications of the author that were imbedded within this dissertation are listed below in a consecutive order, followed by further publications as first author and co-author.

Publications imbedded into this dissertation

- **P1: Stock, S.**; Ceruti, A.; Günter, F. J.; Reinhart, G. (2021). Introducing inline process and product analysis for the lean cell finalization in lithium-ion battery production. Procedia CIRP, 104, 1052-1058, https://doi.org/10.1016/j.procir.2021.11.177.
- **P2: Stock, S.**; Diller, F.; Böhm, J.; Hille, L.; Hagemeister, J.; Sommer, A.; Daub, R. (2023). Operando Analysis of the Gassing and Swelling Behavior of Lithium-ion Pouch Cells during Formation. Journal of The Electrochemical Society, 170(6), 060539, https://doi.org/10.1149/1945-7111/acde0f.
- **P3: Stock, S.**; Ahmed, M.; Konwitschny, F.; Daub, R. (2024). Data Mining for Early Cycle Life Prediction in Lithium-Ion Battery Production. Procedia CIRP, 126, 835-840, https://doi.org/10.1016/j.procir.2024.08.267.
- **P4: Stock, S**.; Pohlmann, S.; Guenter, F. J.; Hille, L.; Hagemeister, J.; Reinhart, G. (2022). Early quality classification and prediction of battery cycle life in production using machine learning. Journal of Energy Storage, 50, 104144, https://doi.org/10.1016/j.est.2022.104144.
- **P5: Stock, S.**; Böhm, J.; Ank, M.; Rath, P.; Lienkamp, M.; Daub, R. (2024). Data-driven approaches for the fast formation of lithium-ion pouch cells using operando gassing analysis. Journal of Power Sources, 613, 234858, https://doi.org/10.1016/j.jpowsour.2024.234858.

Further publications as first author

- **Stock, S.**; Hagemeister, J.; Grabmann, S.; Kriegler, J.; Keilhofer, J.; Ank, M.; Dickmanns, J. L.; Schreiber, M.; Konwitschny, F.; Wassiliadis, N.; Lienkamp, M.; Daub, R. (2023). Cell teardown and characterization of an automotive prismatic LFP battery. Electrochimica Acta, 471, 143341, https://doi.org/10.1016/j.electacta.2023.143341.
- **Stock, S.;** Diller, F.; Daub, R. (2022). Evaluating the Gassing and Swelling Behavior of Lithium-Ion Pouch Cells Using in-Situ Pressure Analysis. In Electrochemical Society Meeting Abstracts 241 (No. 2, pp. 438-438). The Electrochemical Society, Inc, https://doi.org/10.1149/MA2022-012438mtgabs.

Publications as co-author

- Kriegler, J.; Hille, L.; **Stock, S.**; Kraft, L.; Hagemeister, J.; Habedank, J. B.; Jossen, A.; Zaeh, M. F. (2021). Enhanced performance and lifetime of lithium-ion batteries by laser structuring of graphite anodes. Applied Energy, 303, 117693, https://doi.org/10.1016/j.apenergy.2021.117693.

- Hille, L.; Xu, L.; Keilhofer, J.; **Stock, S.**; Kriegler, J.; Zaeh, M. F. (2021). Laser structuring of graphite anodes and NMC cathodes–Proportionate influence on electrode characteristics and cell performance. Electrochimica Acta, 392, 139002, https://doi.org/10.1016/j.electacta.2021.139002.

- Binder, M.; Kuenzel, M.; Diemant, T.; Jusys, Z.; Behm, R.; Binder, J.; **Stock, S.**; Diller, F.; Daub, R.; Bresser, D.; Passerini, S. (2022). A Ternary Additive Mixture for Suppressed Electrolyte Decomposition and Mitigated Gassing in 5V LNMO‖Graphite Li-Ion Cells. In Electrochemical Society Meeting Abstracts 242 (No. 3, pp. 204-204). The Electrochemical Society, Inc, https://doi.org/10.1149/MA2022-023204mtgabs.

- Hille, L.; Noecker, M. P.; Ko, B.; Kriegler, J.; Keilhofer, J.; **Stock, S.**; Zaeh, M. F. (2023). Integration of laser structuring into the electrode manufacturing process chain for lithium-ion batteries. Journal of Power Sources, 556, 232478, https://doi.org/10.1016/j.jpowsour.2022.232478.

- Hagemeister, J.; **Stock, S.**; Linke, M.; Fischer, M.; Drees, R.; Kurrat, M.; Daub, R. (2023). Lean Cell Finalization in Lithium-Ion Battery Production: Determining the Required Electrolyte Wetting Degree to Begin the Formation. Energy Technology, 11(5), 2200686, https://doi.org/10.1002/ente.202200686.

- Ank, M.; **Stock, S.**; Wassiliadis, N.; Burger, T.; Daub, R.; Lienkamp, M. (2023). Influence analysis of production defects of lithium-ion cells using single-cell and multi-cell characterization. Journal of Energy Storage, 62, 106938, https://doi.org/10.1016/j.est.2023.106938.

- Ank, M.; Sommer, A.; Gamra, K. A.; Schöberl, J.; Leeb, M.; Schachtl, J.; Streidel, N.; **Stock, S.**; Bilfinger, P.; Allgäuer, C.; Rosner, P.; Hagemeister, J.; Rößle, M.; Daub, R.; Lienkamp, M. (2023). Lithium-Ion Cells in Automotive Applications: Tesla 4680 Cylindrical Cell Teardown and Characterization. Journal of The Electrochemical Society, 170(12), 120536, https://doi.org/10.1149/1945-7111/ad14d0.

- Lechtenfeld, C. T.; Buchmann, J.; Hagemeister, J.; Bela, M. M.; van Wickeren, S.; **Stock, S.**; Daub, R.; Wiemers-Meyer, S.; Winter, M.; Nowak, S. (2024). Analyzing the Effect of Electrolyte Quantity on the Aging of Lithium-Ion Batteries. Advanced Science, 11(39), 2405897, https://doi.org/10.1016/j.jpowsour.2024.236073.

- Stumper, B.; Wittmann, O.; Diller, F.; **Stock, S.**; Daub, R. (2024). Direct Contact Prelithiation of Multi-Layered Lithium-Ion Battery Pouch Cells Using a Scalable Prelithiation Process. Journal of The Electrochemical Society, 171(12), 120510, https://doi.org/10.1149/1945-7111/ad92e2.

- Binder, M.; Kuenzel, M.; Diemant, T.; Jusys, Z.; Behm, R.; Binder, J.; **Stock, S.**; Diller, F.; Daub, R.; Passerini, S.; Bresser, D. (2025). Ternary electrolyte additive mixture for 5V lithium-ion battery cells. Journal of Power Sources, 630, 236073, https://doi.org/10.1016/j.jpowsour.2024.236073.